Noninvasive Evaluation of Local Myocardial Thickening and Its Color-Coded Imaging

Hiroshi Kanai, *Member, IEEE*, Hideyuki Hasegawa, Noriyoshi Chubachi, *Member, IEEE*, Yoshiro Koiwa, and Motonao Tanaka

Abstract—**For the noninvasive diagnosis of heart disease based on the acoustic characteristics of the heart muscle, we have developed a new method for accurately tracking the movement of the heart wall. By this method, a *velocity signal* of the heart wall with a small amplitude of less than 10 μm on the *motion* resulting from a heartbeat with large amplitude of 10 mm can be successfully detected with sufficient reproducibility in the frequency range up to several hundred Hertz continuously for periods of about 10 heartbeats. In this paper, the method is applied to multiple points preset in the left ventricular (LV) wall along the ultrasonic beam so that the spatial (depth) distributions of the velocity at these points are simultaneously obtained. The motion of the heart wall is divided into the following two components: *parallel global motion* of the heart wall and *the change in myocardial layer thickening* at each depth across the LV wall during *myocardial contraction/relaxation*. The latter component is superimposed on the M (motion)-mode image using a color code to map contraction as red and expansion as blue. By preliminary human studies, the principle of the method proposed in this paper is verified and the frequency band of the components generated by thickening and/or thinning in the myocardium is identified. This new approach offers potential for research on noninvasive acoustical diagnosis of *myocardial local motility*, that is, the myocardial layer function at each depth in the ventricular wall.**

I. Introduction

We herein consider the detection of velocity signals $\{v(x_i;t)\}$ at multiple points $\{i\}$ preset in the LV wall as illustrated in Fig. 1(a) using ultrasound from the chest wall, where the symbol $\{\cdot\}$ denotes the set employed in this paper. The instantaneous position in the depth direction of the ith point set in the LV wall is denoted by $x_i(t)$ as shown in Fig. 1(b). The component of the motion *parallel* to the ultrasonic beam is shown in Fig. 1(c). The parallel components at all points along the ultrasonic beam in Fig. 1(c) are the same in phase and magnitude if the beam is perpendicular to the heart wall. The LV wall motion during the cardiac cycle is much larger in magnitude compared with the thickness change. The LV wall shows periodic thickening and thinning along with *myocardial contraction and relaxation* as illustrated in Figs. 1(b) and (d). The difference between position $x_i(t)$ of the ith point and position $x_{i+1}(t)$ of the $(i+1)$th point shows the local thickness at every instant of time during one cardiac cycle as shown in Fig. 1(d). The thickness change corresponds to the local motility of the myocardial layer across the LV wall, possibly an essential diagnostic tool for heart diseases.

To establish this noninvasive method for the local characteristics across the LV wall using ultrasound, accuracy

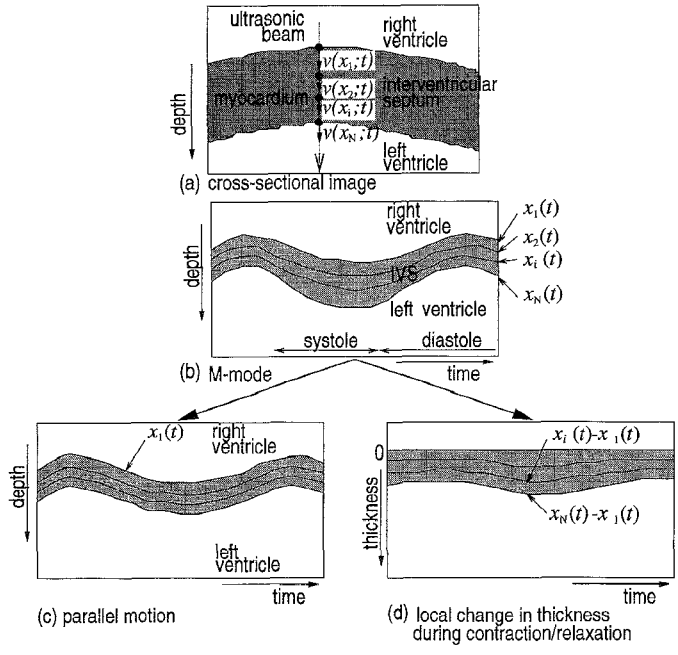

Fig. 1. An illustration explaining the process of the evaluation of the local change in thickness during myocardial contraction/relaxation based on noninvasive detection of velocity signals $\{v(x_i;t)\}$ and the instantaneous positions $\{x_i(t)\}$ of multiple N points $\{i\}$ in the heart wall. (a): Cross-sectional image of the heart wall. (b): Tracking results $\{x_i(t)\}$ for multiple N points $\{i\}$ in the heart wall, shown in the same form as in the M-mode image. $x_i(t)$ shows the instantaneous position in the depth direction of the ith point preset in the heart wall, where $i = 1, 2, \ldots, N$. (c) and (d): Tracking results $\{x_i(t)\}$ are divided into the parallel motion $x_1(t)$ in (c) and the local change in thickness $\{x_i(t) - x_1(t)\}$ during myocardial contraction/relaxation in (d). From the latter spatial distribution, the instantaneous local change in thickness, which corresponds to the myocardial local motility, is evaluated and displayed in a color-coded image in this paper.

Manuscript received June 3, 1996; accepted December 16, 1996. This work was supported in part by a Grant-in-Aid for Scientific Research from the Ministry of Education, Science and Culture of Japan.

H. Kanai, H. Hasegawa, and N. Chubachi are with the Department of Electrical Engineering, Faculty of Engineering., Tohoku University, Sendai 980-77, Japan (e-mail: hkanai@chubachi.ecei.tohoku.ac.jp).

Y. Koiwa is with the First Department of Internal Medicine, School of Medicine, Tohoku University, Sendai 980-77, Japan.

M. Tanaka is with the Tohoku Welfare Pension Hospital, Takasago 10, Fukumuro, Miyagino-ku, Sendai 983, Japan.

0885-3010/97$10.00 © 1997 IEEE

required in the simultaneous measurement of the instantaneous positions $\{x_i(t)\}$ of the multiple points $\{i\}$ in the heart wall is estimated as follows. For the interventricular septum (IVS), for example, the thickness is about 10 mm for a normal young adult and the change in thickness is approximately 1 mm to 3 mm during one cardiac cycle [1]. Thus, when the distance between points (i) and $(i+1)$ is 0.75 mm, the minimum value of the thickness change between these points is approximately 75 μm. For the evaluation of local myocardial motility, therefore, 10 μm is employed as the necessary spatial resolution in the measurement of instantaneous position. If the velocity signal $v(x_i;t)$ of the ith preset point is detected based on the pulse Doppler method, necessary accuracy of the velocity measurement is about 10 μm/200 μs = 0.05 m/s when the pulse repetition frequency (PRF) of the transmission-pulse train is 5 kHz (= 1/200 μs). If the equivalent sampling period of the velocity signal $v(x_i;t)$ is longer than 200 μs as in the standard color Doppler system, for example, more accurate velocity measurement is required. Since there is motion with large amplitude (about $\pm$10 mm) caused by the heartbeat as described above, moreover, the dynamic range required in the measurement of the displacement is about 1000 (= 10 mm/10 μm) = 60 dB in amplitude.

M-mode echocardiography offers an advantage in critically looking at the motion pattern of the left ventricle because of the increased frequency of sampling. However, its spatial resolution along the ultrasonic beam is limited to a few wavelengths, namely, only up to 1 mm for ultrasound of 3 MHz. Moreover, to detect the displacement of point (i) as waveform as shown in Fig. 1(b) to be analyzed, it is necessary to accurately identify its instantaneous position $x_i(t)$ and to trace the resultant displacement. However, this is not easily realized in M-mode echocardiography. On the other hand, numerous elaborate techniques have been proposed for noninvasive measurement of the velocity of the blood flow in the heart or the arteries based on the Doppler effect [2]–[11]. Moreover, several methods, including the PLL techniques, have been developed to measure changes in the diameter of the arterial walls by tracking arterial wall displacement including only low frequency components with small amplitudes [12]–[31]. However, transcutaneous and accurate detection of the velocity signal on or in the heart wall has not yet been established.

We have proposed, therefore, a noninvasive transcutaneous method for detecting small *velocity* signals on the surface of the heart wall [1], [32]. By calculating the constraint cross-correlation function between the sequentially received echoes, the phase change caused by displacement of the ith preset point during the pulse repetition period ΔT is accurately determined and the average velocity $v(x_i;t)$ during the period is obtained. By adding the product of $v(x_i;t)$ and ΔT to the previous object position $x_i(t)$, the next position $x_i(t+\Delta T)$ is estimated. The detected velocity signal shows rapid motion of the heart wall including high frequency components with small amplitudes, which are difficult to recognize by M-mode echocardiography. The validity of the proposed method has been confirmed by experiments using a water tank and has been applied to the *in vivo* detection of small *velocity* signals, with sufficient reproducibility, on the wall of the human heart [1]. Spectrum analysis was first applied to the resultant noninvasively detected signals to show the possibility of acoustic diagnosis of the heart wall [1]. However, it corresponds to *the global evaluation* of the heart wall because the detected velocity signals have not been divided into the *parallel and thickness change components*, and the latter component is much less than the former one.

In this paper, the method is applied to multiple points preset along an ultrasonic beam in the LV wall so that the instantaneous object positions $\{x_i(t)\}$ and the velocity signals $\{v(x_i;t)\}$ are obtained for these multiple points $\{i\}$ in the LV wall. From the spatial distributions of $\{x_i(t)\}$ and $\{v(x_i;t)\}$ in the direction of depth, the motion of the LV wall is divided into the *parallel component* $x_1(t)$ as shown in Fig. 1(c) and the *thickness change components* $\{x_i(t)-x_{i-1}(t)\}$ *during myocardial contraction/relaxation*, as shown in Fig. 1(d). From the latter component, the spatial distribution of the normalized local change in thickness of the heart wall is obtained and is superimposed on the M-mode image using a color code. The principle is confirmed by the preliminary *in vivo* experiments herein reported. By applying spectrum analysis to the velocity signals, the frequency band for the component due to the myocardial thickening and thinning is identified.

II. Principle of Accurate Measurement of Instantaneous Position and Velocity in the Myocardium

From observation of the standard echo cardiography, it can be assumed that there are many objects along the ultrasonic beam in the heart wall which reflect the transmitted ultrasonic pulse. Thus, we manually preset multiple N points $\{i\}$ in the heart wall at a time t_0 in one cardiac cycle by referring to the M-mode image. In this paper, we assume that each point of $\{i\}$ has a velocity component which is parallel to the direction of this beam if the direction and position of the ultrasonic beam are appropriately selected so that it is perpendicular to the wall of the heart during the cardiac cycle. The principle of the accurate detection of the instantaneous positions $\{x_i(t)\}$ and velocity signals $\{v(x_i;t)\}$ of multiple points $\{i\}$ in the heart wall is briefly described as follows by referring to [1].

A. Measurement of Object Velocity $v(x_i;t)$

RF pulses with angular-frequency $\omega_0 = 2\pi f_0$ are transmitted at a time interval of ΔT from an ultrasonic transducer on the chest surface as illustrated in Fig. 2. Defining the acoustic velocity as c_0, the instantaneous distance of a object point (i) from the ultrasonic transducer is denoted by $x_i(t) = c_0 \cdot \tau_i(t)$, where $\tau_i(t)$ is the instantaneous period required for one-way transmission from the ultrasonic transducer to the object (i). The ultrasonic pulse

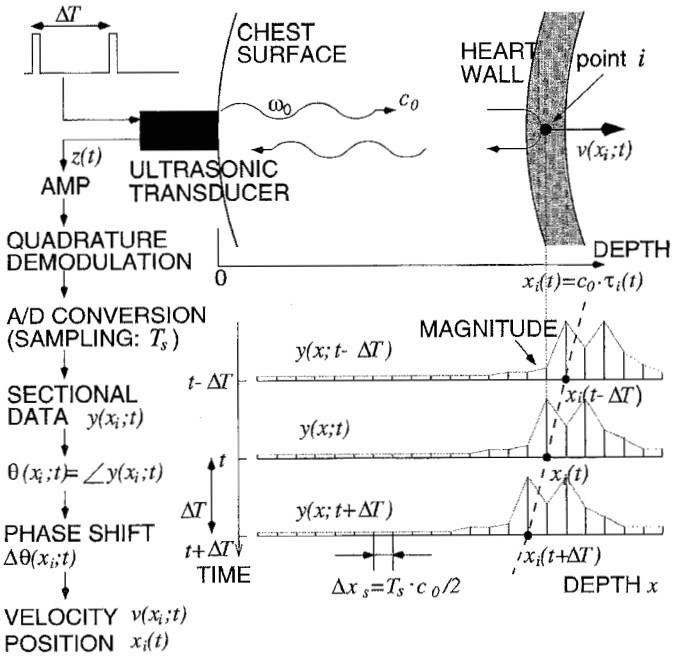

Fig. 2. Schematic representation of the principle of the transcutaneous detection of a velocity signal $v(x_i,t)$ and the instantaneous position $x_i(t)$ of the ith point in the heart wall using pulsed ultrasound from the chest wall.

reflected by the object (i) is received by the same ultrasonic transducer. The output signal, $z(t)$, is amplified and quadrature-demodulation is applied to the signal. The resultant in-phase and quadrature signals are simultaneously A/D converted at a sampling period of T_S, and these two signals are combined into a complex signal, which is termed an *analytic signal*. The analytic signal is then separated into the response signals $\{y(x_i;t)\}$ for each transmitted pulse, where $x_i(t)$ and its simple expression x_i denote the depth of the object (i) from the ultrasonic transducer. The spatial resolution Δx_S in the depth direction is equal to $T_S \cdot c_0/2$ as shown in Fig. 2.

The phase $\theta(x_i;t)$ of the resultant sectional analytic signal $y(x_i;t)$ is given by the angular frequency ω_0 multiplied by twice the delay time $\tau_i(t)$ in the one-way propagation from the ultrasonic transducer to the object. Thus, the phase difference $\Delta\theta(x_i;t)$ between the analytic signals $y(x_i;t)$ and $y(x_i;t+\Delta T)$ of the received signals for the successively transmitted pulses in the interval ΔT is given by

$$\begin{aligned}\Delta\theta(x_i;t) &= \theta(x_i;t+\Delta T) - \theta(x_i;t)\\ &= 2\omega_0\{\tau_i(t+\Delta T) - \tau_i(t)\}\\ &= \frac{2\omega_0}{c_0}\Delta x_i(t),\end{aligned} \tag{1}$$

where $\Delta x_i(t) = x_i(t+\Delta T) - x_i(t)$ is the movement of the object (i) in the period ΔT after a time t, where it can be assumed that the received interval almost coincides with the transmitted interval ΔT of the ultrasonic RF pulses. By dividing the movement $\Delta x_i(t)$ by the period ΔT, the average velocity, denoted by $\widehat{v}(x_i;t+\frac{\Delta T}{2})$, of the object during the period ΔT around the time $t+\Delta T/2$ is given by the phase difference $\Delta\theta(x_i;t)$ between the successively received analytic signals $y(x_i;t)$ and $y(x_i;t+\Delta T)$ as follows [11]:

$$\begin{aligned}\widehat{v}\left(x_i;t+\frac{\Delta T}{2}\right) &= \frac{\Delta x_i(t)}{\Delta T}\\ &= c_0 \cdot \frac{\Delta\theta(x_i;t)}{2\omega_0 \cdot \Delta T}. \quad [\mathrm{m/s}]\end{aligned} \tag{2}$$

B. Accurate Determination of the Phase Change $\Delta\theta(x_i;t)$

Since it is essential to accurately determine the phase change $\Delta\theta(x_i;t)$ of (2) during the period ΔT, the following complex correlation is introduced in the determination procedure of the movement, δ_x, of the object position $x_i(t)$ from the data of the preceding section during the period ΔT.

Based on the least squares method, we define the normalized mean squared difference between the analytic signal $y(x_i+\delta_x;t+\Delta T)$ and the preceding signal $y(x_i;t)$ by $\alpha_n(\beta_n;\delta_x)$,

$$\alpha_n(\beta_n;\delta_x) = \frac{\sum_{x=x_i(t)-\Delta x}^{x_i(t)+\Delta x} |y(x+\delta_x;t+\Delta T) - \beta_n(\delta_x;x_i;t)y(x;t)|^2}{\sum_{x=x_i(t)-\Delta x}^{x_i(t)+\Delta x} \frac{1}{2}\left\{|y(x+\delta_x;t+\Delta T)|^2 + |y(x;t)|^2\right\}},$$

where δ_x is the movement, to be determined, of the object i during the period ΔT of the consecutive echoes and $\beta_n(\delta_x;x_i;t)$ is the average change from the analytic signal $y(x;t)$ to $y(x+\delta_x;t+\Delta T)$ around $x_i(t)$ and is a function of δ_x, $x_i(t)$, and t. The range from $x_i(t)-\Delta x$ to $x_i(t)+\Delta x$ around the previous object-position $x_i(t)$ is the period where the above difference is evaluated and the range $2\Delta x$ corresponds to the length of the RF pulse transmitted from the ultrasonic transducer. The denominator of (3) shows the average power of these analytic signals around $x_i(t)$, which normalizes the mean squared difference of the numerator.

From the theoretical consideration [1], the optimum value of β_n by which the minimum of $\alpha_n(\beta_n;\delta_x)$ is given coincides with the β_n which maximizes the magnitude of the standard complex cross-correlation function between $y(x;t)$ and $y(x;t+\Delta T)$ in the range around $x_i(t)$.

When the received complex signals $y(x;t)$ and $y(x;t+\Delta t)$ are described by the damped sinusoidal signals, however, the above standard cross-correlation procedure does not uniquely determine the optimum movement δ_x of the signal $y(x;t+\Delta t)$ from $y(x;t)$ as theoretically described in [1]. To solve the above problem, by restricting the magnitude of $\beta_n(\delta_x;x_i;t)$ in (3) to one and replacing $\beta_n(\delta_x;x_i;t)$ by $\exp(j\Delta\theta(\delta_x;x_i;t))$, we redefine the normalized mean squared difference $\alpha(\Delta\theta;\delta_x)$ of (3) between

$y(x_i+\delta_x;t+\Delta T)$ and $y(x_i;t)$ by $\alpha(\Delta\theta;\delta_x)$:

$$\alpha(\Delta\theta;\delta_x) = \frac{\sum_{x=x_i(t)-\Delta x}^{x_i(t)+\Delta x} \left|y(x+\delta_x;t+\Delta T) - e^{j\Delta\theta(\delta_x;x_i;t)}y(x;t)\right|^2}{\sum_{x=x_i(t)-\Delta x}^{x_i(t)+\Delta x} \frac{1}{2}\left\{|y(x+\delta_x;t+\Delta T)|^2 + |y(x;t)|^2\right\}},$$

where $\Delta\theta(\delta_x;x_i;t)$ is the phase change from $y(x;t)$ to $y(x+\delta_x;t+\Delta T)$ around $x_i(t)$ and is a function of δ_x, $x_i(t)$, and t. The minimization of $\alpha(\Delta\theta;\delta_x)$ is achieved by:

$$\exp(j\widehat{\Delta\theta}) = \frac{\sum_{x=x_i(t)-\Delta x}^{x_i(t)+\Delta x} y^*(x;t)\cdot y(x+\delta_x;t+\Delta T)}{\left|\sum_{x=x_i(t)-\Delta x}^{x_i(t)+\Delta x} y^*(x;t)\cdot y(x+\delta_x;t+\Delta T)\right|}. \quad (3)$$

For this value of $\exp(j\widehat{\Delta\theta})$, the minimum $\alpha_{MIN}(\delta_x)$ of $\alpha(\widehat{\Delta\theta};\delta_x)$ with respect to $\widehat{\Delta\theta}$ is uniquely given. By introducing the restriction, a solution different from the complex cross-correlation function derived from the nonrestricted definition in (3) is obtained [1]. From the phase change $\widehat{\Delta\theta}(\widehat{\delta_x};x_i;t)$ and $\widehat{\delta_x}$ by which minimization of $\alpha(\Delta\theta;\delta_x)$ in (3) is achieved, the average velocity in (2) is given by:

$$\widehat{v}\left(x_i;t+\frac{\Delta T}{2}\right) = c_0\cdot\frac{\widehat{\Delta\theta}(\widehat{\delta_x};x_i;t)}{2\omega_0\cdot\Delta T}. \quad [\text{m/s}] \quad (4)$$

C. Tracking the Object Position $x_i(t)$

The position $x_i(t)$ of the object (i) in the heart wall changes by more than 10 mm due to the heartbeat in one cardiac cycle. It is, therefore, necessary to accurately track the instantaneous object position $x_i(t)$ in order to estimate the velocity signal $v(x_i;t)$ of the object (i). For this purpose, by multiplying the velocity estimate $\widehat{v}(x_i;t+\frac{\Delta T}{2})$ of (4) by the period ΔT, the next object position $\widehat{x}_i(t+\Delta T)$ is estimated by:

$$\widehat{x}_i(t+\Delta T) = \widehat{x}_i(t) + \widehat{v}\left(x_i;t+\frac{\Delta T}{2}\right)\cdot\Delta T. \quad [\text{m}] \quad (5)$$

Thus, the resultant object position $\widehat{x}_i(t)$ and the velocity $\widehat{v}(x_i;t+\frac{\Delta T}{2})$ are simultaneously determined.

The quadrature-demodulated signals are A/D converted at a sampling interval of T_S. When the velocity is assumed to be 5 mm/s, for example, and the time interval ΔT of the transmission of the RF pulses is 200 μs, the displacement $\Delta x_i(t) = x_i(t+\Delta t) - x_i(t)$ of the object (i) is 2 μm during the time interval ΔT, which is much less than the spatial resolution $\Delta x_S = T_S \times c_0/2 = 750$ μm of Fig. 2 in the depth direction when the sampling period T_S is 1 μs. As shown in this example, the resultant estimate $\widehat{x}_i(t)$ of the next object position in (5) is represented not by a discrete value but by the continuous value in the above procedure because the instantaneous velocity $v(x_i;t)$ is given by the phase difference $\Delta\theta(x_i;t)$ in (2). Thus, accurate tracking of the object is realized by this method, which is confirmed by the experiments in Section V.

III. Principle of the Measurement of Thickness Change in the Myocardium

By applying the above method to each of the multiple N points in the heart wall, the instantaneous object positions $x_i(t)$, and the velocity signals $v(x_i;t)$ are obtained for $i = 1,2,\ldots,N$ as shown in Fig. 1(b). At the beginning of this procedure, the initial positions (depth) $\{x_i(t_0)\}$ of the N points $\{i\}$ at a time t_0 are manually preset at even intervals of Δx_S along the ultrasonic beam in the heart wall, where Δx_S is the spatial resolution in the depth direction. We employ the time t_0 at 200 ms before the first R-wave during the A/D conversion, regarding it as near the end-diastole. Thus, the initial positions are given by:

$$x_i(t_0) = x_1(t_0) + \Delta x_S \times (i-1), \quad (6)$$

where $i = 1,2,\ldots,N$. For example, for the presetting of the initial positions in the IVS with reference to the longitudinal M-mode image, $x_1(t_0)$ and $x_N(t_0)$ correspond to the position on the surface of the right ventricle (RV) and the surface of the left ventricle (LV) of the IVS, respectively. For the setting in the LV posterior wall, $x_1(t_0)$ and $x_N(t_0)$ correspond to the positions on the endocardium and the epicardium in the wall, respectively.

Let us assume that the ultrasonic beam is perpendicular to the heart wall during one cardiac cycle as shown in Fig. 1(a) and that the velocity direction of each point i in the heart wall is parallel to the direction of the ultrasonic beam. Thus, from the difference between the instantaneous object position $x_i(t)$ and the instantaneous position $x_{i+1}(t)$ of the sequentially set point, the *thickness* of the local region between points (i) and $(i+1)$, which is denoted by $h_i(t)$, is obtained by:

$$h_i(t) = x_{i+1}(t) - x_i(t) > 0. \quad [\text{m}] \quad (7)$$

Since the depth axis of Fig. 1(b) is positive in the downward direction, the thickness $h_i(t)$ in (7) is always positive as shown in Fig. 1(d).

On the other hand, from the difference between the velocity values $v(x_i;t)$ and $v(x_{i+1};t)$, the *instantaneous speed* $\Delta_t h_i(t)$ *of the local change in thickness* is obtained by:

$$\Delta_t h_i(t) = v(x_{i+1};t) - v(x_i;t). \quad [\text{m/s}] \quad (8)$$

When the region between the ith and $(i+1)$-th points become thicker at a time t, $\Delta_t h_i(t) > 0$, while for the case when the region become thinner, $\Delta_t h_i(t) < 0$. However, $\Delta_t h_i(t)$ depends on the distance between $x_i(t)$ and $x_{i+1}(t)$. Thus, by dividing $\Delta_t h_i(t)$ by the distance $|x_{i+1}(t) - x_i(t)|$, the *normalized speed of the local change in thickness* which

occurs in the assumed homogeneous myocardium between points (i) and $(i+1)$, denoted by $S_i(t)$, is defined by:

$$S_i(t) = \frac{\Delta_t h_i(t)}{|x_{i+1}(t) - x_i(t)|}. \quad [(\mathrm{m/s})/\mathrm{m}] \tag{9}$$

In actual *in vivo* measurement for the IVS, for example, the typical values of $\Delta_t h_i(t)$ and $|x_{i+1}(t) - x_i(t)|$ are 4 mm/s and 0.75 mm, respectively. For these values, $S_i(t)$ of (9) is 5.3 [(mm/s)/mm]. By multiplying an appropriate short period δT_0 and the thickness of the region by the numerator in the right-hand side of (9), the thickness change which occurs in the region per period δT_0 is estimated. Thus, $S_i(t)$ of (9) yields a generalized form because $S_i(t)$ does not depend on the PRF nor on the spatial resolution Δx_S directly determined by the sampling period T_S in the A/D conversion.

The spatial distributions $\{S_i(t)\}$ of the normalized speed of the local change in thickness are color coded and superimposed on the M-mode image. In this paper, *red* corresponds to thinning of the myocardium ($S_i(t) < 0$) and *blue* corresponds to thickening of the myocardium ($S_i(t) > 0$) as shown in Fig. 6(1-d). The color scheme corresponds to the temperature increase due to the adiabatic contraction and the temperature decrease due to the adiabatic expansion, respectively. This color scheme differs from that employed in standard color Doppler imaging [11] or tissue Doppler imaging [35]–[37] because the color coding in those systems is determined not by the speed of the local change in thickness but by the estimated local instantaneous velocity.

IV. A System for Measurement and Analysis

In order to realize the procedure proposed in Sections II and III, a high speed A/D converter with a large-scale memory and an engineering workstation are employed to analyze the analytic signal, $y(t)$, resulting from the quadrature-modulation of the signal $z(t)$ received by the sector-type ultrasonic transducer of the standard ultrasonic diagnostic equipment (Toshiba SSH-160A). In the diagnostic equipment, the standard B-mode cross-sectional image and M-mode image are displayed to identify the measurement points on the heart wall. The frequency f_0 of the transmitted ultrasound and repetition interval ΔT=(1/PRF) of the transmission of the ultrasonic pulses are set at 3 MHz and 222 μs, respectively, in the experiments in the following sections. At these conditions, the upper limit $|v_{max}|$ of the velocity measurement, which is free from the aliasing effect, is given by:

$$|v_{max}| = \frac{c_0}{4 f_0 \Delta T} = 0.462 \text{ m/s}, \tag{10}$$

when the acoustic speed c_0 is assumed to be 1540 m/s. The upper limit is much greater than the velocity of the LV wall.

The signal, $z(t)$, received by the ultrasonic transducer is amplified and quadrature-demodulated by the ultrasonic diagnostic equipment. The resultant in-phase signal and the quadrature signal are simultaneously A/D converted with a 2-channel 12-bit A/D converter at a sampling rate of $1/T_S$. The sampling rate $1/T_S$ in the system is variable from 1 MHz to 10 MHz; 1 MHz is employed in the following experiments. Thus, the spatial resolution $\Delta x_S = T_S \cdot c_0/2$ in the depth direction is about 0.75 mm. In the A/D converter employed, the length of each signal is limited to 1,046,000 points ($\simeq$ 1 Mega words). However, these two signals are digitized only for the period of length T_0 where at least the signals reflected at the N points are received by the ultrasonic transducer. Thus, the effective length of the digital signal in the A/D converter is increased from 1 second ($=$ 1 Mega $\times\, T_S$) to several seconds ($=$ 1 Mega $\times\, T_S \times \Delta T/T_0$), that is, several heartbeat periods because the typical values of ΔT and T_0 are 222 μs and 35 μs, respectively, for the experiments in this paper. For this intermittent digitization, a sampling clock of 1 MHz is generated only for the period T_0 by an external signal generator, which is completely synchronous with the master clock of the ultrasonic diagnostic equipment. The electrocardiogram (ECG) and phonocardiogram (PCG) are also digitized so that their acquisition timing is synchronous with that of the ultrasonic wave transmission from the transducer. Then, the proposed method described in Sections II and III is applied to the resultant digital signals, which are transferred from the A/D converter to the workstation via a GPIB interface. Each resultant velocity signal $v(x_i; t)$ obtained by the proposed method is passed through the digital low-pass filter with a cut-off frequency f_c of 600 Hz, which is realized by the finite impulse response (FIR) filter of the Hamming window with a length of 3.3 ms.

V. Experimental Evaluation of Measurable Lower Limit Using Water Tank

In a previous paper [1], the principle of the method proposed in Section II was confirmed using a water tank which simulated the small vibration of the ventricle wall on the motion with large amplitude of $\pm$7.5 mm caused by the heartbeat. Briefly, for large amplitude motion caused by the eccentric cam in the water tank, the tracking result of the surface of the rubber plate exactly coincided with the M-mode image. For small vibration with a peak-to-peak amplitude of about 20 μm generated by a small vibrator on the eccentric cam, evaluation using the squared-magnitude of the coherence function showed that the small velocity signal on the large motion was successfully detected in the frequency range from 1 to 1000 Hz.

In this paper, in addition to the above experiments, the lower limit of the measurable velocity and the thickness change is evaluated using a rubber plate fixed in a water tank. The longitudinal velocity c_0 in the rubber is about 1.5×10^3 m/s. The measurement system described in Section IV is employed with the same values for the parameters of f_0, ΔT, T_S, and f_c.

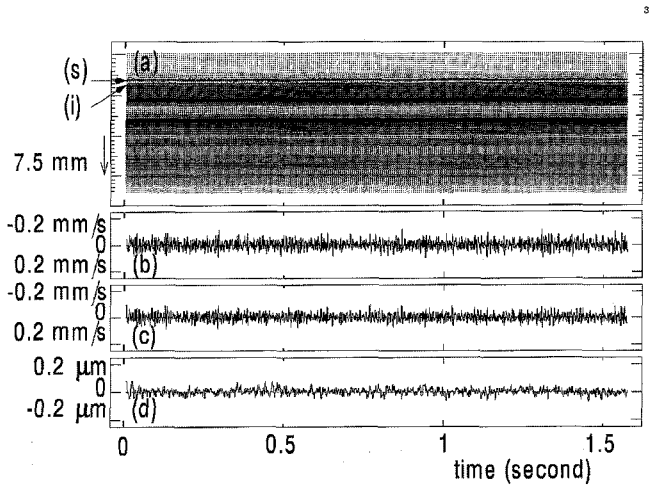

Fig. 3. Experimental results for evaluation of measurable lower limit using a water tank. (a): The object motion $x_s(t)$ and $x_i(t)$ estimated by the proposed method, superimposed on the M-mode image obtained by the magnitude of the received signal. (b) and (c): The velocity signal estimates $v(x_s;t)$ and $v(x_i;t)$ of points (s) and (i). (d): The change in thickness, $h(t)$, between point (i) and (s) obtained from $v(x_s;t)$ and $v(x_i;t)$.

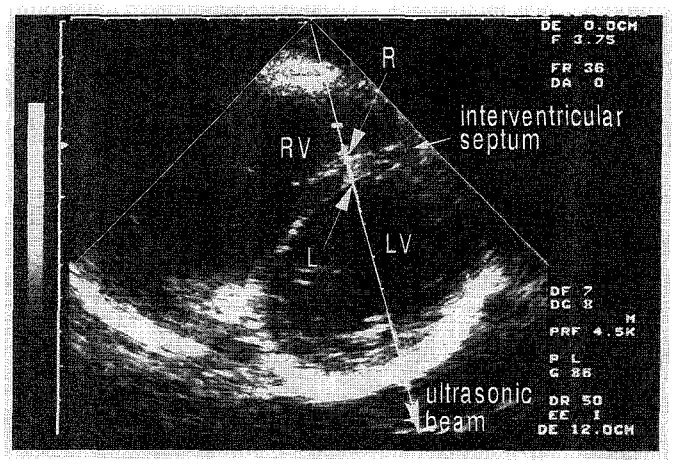

Fig. 4. A standard B-mode short-axis image showing the cross-sectional area around the detected points preset in the interventricular (IVS) in an *in vivo* experiment for the detection of their instantaneous positions and the velocity signals of a presumedly healthy 26-year-old male volunteer. Points (R) and (L) are on the RV surface and the LV surface of the IVS, respectively. The ultrasonic beam passing through the two points is almost perpendicular to the septum during the measurements.

Fig. 3(a) shows the M-mode image obtained from the magnitude of the received signal. The positions $x_s(t)$ and $x_i(t)$ of point (s) on the rubber surface and point (i) in the rubber, respectively, are manually preset at the leftmost timing in Fig. 3(a). The distance between these points is 0.75 mm. The tracking results superimposed in Fig. 3(a) show that $x_s(t)$ and $x_i(t)$ are almost straight lines.

Figs. 3(b) and (c) show that the velocity signals $v(x_s;t)$ and $v(x_i;t)$ at points (s) and (i) obtained by the proposed method. By integrating the difference between $v(x_s;t)$ and $v(x_i;t)$, the change in thickness, $h(t)$, of (7) is obtained as shown in Fig. 3(d).

The vertical axis of Figs. 3(b)-(d) is magnified so that the noise component of each signal can be shown. Each signal should be zero if the signal-to-noise ratio is infinite. From Figs. 3(b) and (d), the lower limit $|v_{min}|$ of the velocity measurement is approximately given by:

$$|v_{min}| = 0.1 \text{ mm/s}, \tag{11}$$

which is less than 1/2000 of the upper limit $|v_{max}| =$ 462 mm/s of the measurable velocity in (10). Since $|v_{max}|$ corresponds to π radian of the phase-shift during the pulse repetition interval ΔT, error in the phase-shift detection is less than 0.04 degree (= 0.1 [mm/s] $\times$ 180°/462 [mm/s]). The dynamic range of the velocity measurement is given by:

$$\text{dynamic range} = 20 \log \left| \frac{v_{max}}{v_{min}} \right| = 73 \text{ dB}. \tag{12}$$

From Fig. 3(d), the lower limit $|h_{min}|$ of the measurement of the change in thickness between these two points (s) and (i) in the developed measurement system is approximately given by:

$$|h_{min}| = 0.1 \quad \mu\text{m}. \tag{13}$$

From these experiments, sufficient accuracy and precision have been confirmed.

VI. *In Vivo* Experimental Results for the Interventricular Septum

A. Explanation of the Procedure of the Proposed Method

The proposed method is applied to the detection of velocity signals on the IVS of a healthy 26-year-old male volunteer. Fig. 4 shows the B-mode image of the LV in the short axis, which was obtained by standard ultrasonic diagnostic equipment. The 14 points $\{i\}$ are set in the region from point (R) on the RV surface to point (L) near the LV side of the IVS, where $x_R(t) = x_1(t)$ and $x_L(t) = x_{14}(t)$. Since the results obtained by the proposed method depend on the angle between the direction of the velocity vector and the ultrasonic beam, the direction of the ultrasonic beam passing through points (R) and (L) is selected so that the beam is on the LV center in the cross-section and is almost perpendicular to the IVS, as shown in Fig. 4, during the A/D conversion of several cardiac cycles. During the acquisition period, respiration is suspended.

Figs. 5(a) and (b) show the ECG and PCG, respectively. Fig. 5(c) shows the M-mode image which was reconstructed from the magnitude of the digitized signal of the analytic signals. Before applying the method described in Section II, by referring to the M-mode image of Fig. 5(c), the positions $\{\widehat{x}_i(t_0)\}$ of the 14 points $\{i\}$ are manually preset using the workstation at even intervals of Δx_S=0.75 mm from point (R) near the surface of the RV side of the IV to point (L) near the surface of the LV

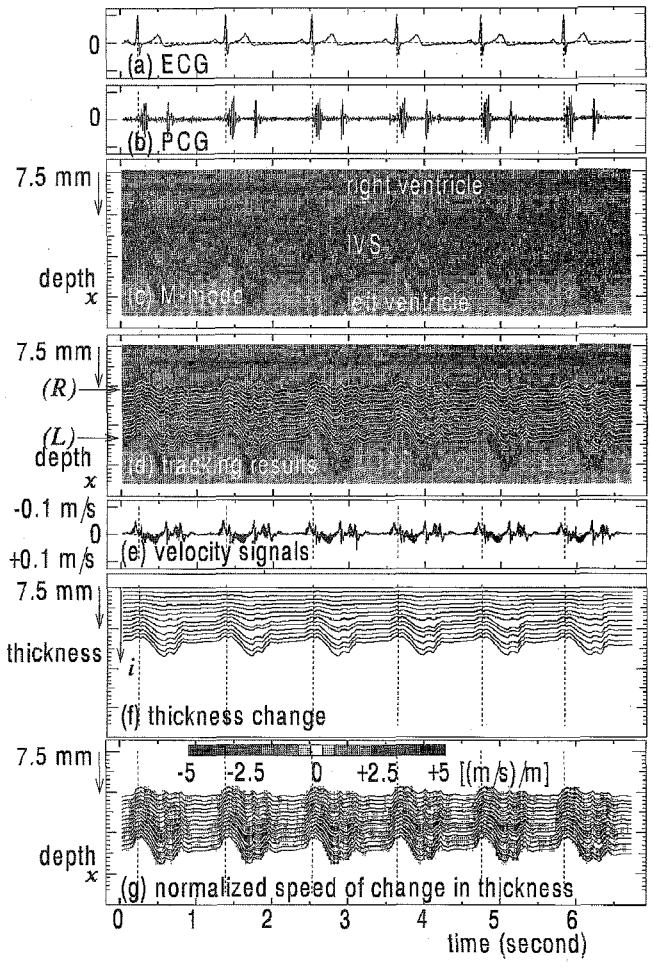

Fig. 5. *In vivo* experimental results of instantaneous object position and velocity estimated at 14 points $\{i\}$ preset in the IVS of the normal young male subject in Fig. 4. (a): ECG. (b): PCG. (c): The M-mode image. (d): The tracking results $\{\widehat{x}_i(t)\}$ in (7) of the 14 points $\{i\}$, which correspond to the illustration of Fig. 1(b). These results are superimposed on the M-mode image in (c). The points (R) and (L) correspond to the surface on the RV side and the surface near the LV side of the IVS, respectively. (e): Superimposed estimates of the velocity signals $\{\widehat{v}(x_i;t)\}$ of the 14 points $\{i\}$ in the heart wall. (f): The change in thickness, $\{\widehat{x}_i(t)-\widehat{x}_1(t)\}$, from the RV side to the ith point in the IVS for $i=1,2,\ldots,14$. (g): The normalized speed of the local change in thickness, $\{S_i(t)\}$ [(m/s)/m], which occurs in the region between points $\{i\}$ and $\{i+1\}$. The absolute values $\{|S_i(t)|\}$ are mapped using black and white and the results are superimposed on the tracking results of (d).

side. The tracking results $\{\widehat{x}_i(t)\}$, estimated by (5) of the 14 points $\{i\}$, are superimposed on the M-mode image as shown in Fig. 5(d).

Fig. 5(e) shows the superimposed estimates of the velocity signals $\{\widehat{v}(x_i;t)\}$ on the tracked points $\{\widehat{x}_i(t)\}$, where $i=1,2,\ldots,14$. The vertical axis of Fig. 5(e) is inverted so that the negative value of the velocity, which is shown above the baseline, corresponds to the situation in which the object moves in the direction of the ultrasonic transducer on the chest wall, which is more easily understood. The resultant vibration signals are sufficiently reproducible for five heartbeat periods.

Fig. 5(f) shows the thickness change, $\{\widehat{x}_i(t)-\widehat{x_1}(t)\}$, that occurs in the region between the point (R) on surface of the RV side and the ith point in the IVS. Each waveform of $\{\widehat{x}_i(t)-\widehat{x_1}(t)\}$ is also almost completely reproducible for the five heartbeat periods. For the systolic phase, the IVS becomes about 3 mm thicker than that of the diastolic phase, where the thickness of the IVS is about 10 mm at the end of the diastole.

Fig. 5(g) shows the normalized speed of the local change in thickness, $\{S_i(t)\}$, of (9), which occurs in the local region between points $\{i\}$ and $\{i+1\}$. In this figure, their absolute values $\{|S_i(t)|\}$ are mapped as black and white and the results are superimposed on the tracking results $\{\widehat{x}_i(t)\}$ of Fig. 5(d). For the region and the timing where there is a large change in thickness in Fig. 5(f), for example, for the beginning and the end of the systole especially at the LV side in the IVS, the instantaneous local change in thickness is found to be large.

B. Color-Coded Imaging

By magnifying the time axis in Fig. 5, Fig. 6(1) shows the results for the first cardiac cycle. Fig. 6(1-d) shows the tracking results $\{\widehat{x}_i(t)\}$ of the 14 points $\{i\}$ by white lines and the normalized speed of the local change in thickness, $\{S_i(t)\}$, of (9). The values $\{S_i(t)\}$ are color coded according to the coloring scheme described in Section III and the results are superimposed on the M-mode image of Fig. 6(1-c). Fig. 6(1-e) shows superimposed estimates of the velocity signals $\{\widehat{v}(x_i;t)\}$ of the 14 points $\{i\}$ in the heart wall. Especially for the period of the beginning of the systole and the beginning of the diastole after the second heart sound (II), there are relatively large differences between the velocity estimates, which correspond to the thickening and thinning, respectively, in the heart wall. For the period around the R-wave and the center of the diastole, however, these velocity estimates coincide with each other, which corresponds to the parallel motion as illustrated in Fig. 1(c). Fig. 6(1-f) shows the change in thickness, $\{\widehat{x}_i(t)-\widehat{x}_1(t)\}$, between the RV side and the ith point in the IVS for $i=1,2,\ldots,14$.

C. Spectrum Analysis of the Velocity Signals

Figs. $\{7(\text{c-}i)\}$ (i=1, 3, 5, 7, 9, 11, 13) separately show each of the velocity signals $\{\widehat{v}(x_i;t)\}$ for 7 of the 14 points of Fig. 5(e). In these figures, the results for the first 5 heartbeats are overlaid and shown. Around the center of the systolic phase, the velocity estimates $\{\widehat{v}(x_i;t)\}$ in the IVS have small positive values for about 200 ms as shown in Fig. 7(c), which means that the IVS slowly moves to the LV. The amplitude of $\widehat{v}(x_1;t)$ of Fig. 7(c-13) on the LV side is a little greater than that of $\widehat{v}(x_R;t)$ of Fig. 7(c-1) on the RV side, especially in the systolic phase. This difference corresponds to the change in thickness due to the expansion in the wall of the IVS.

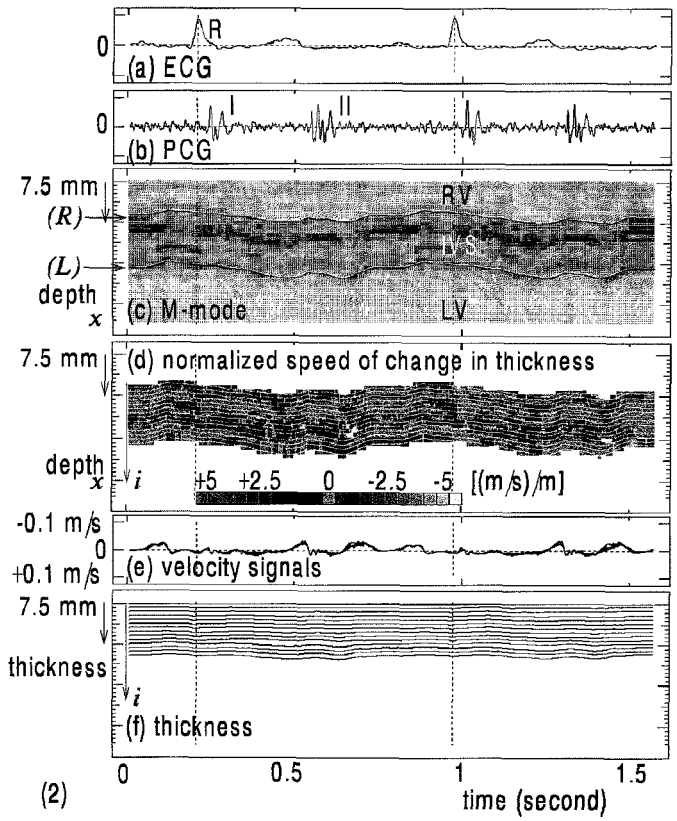

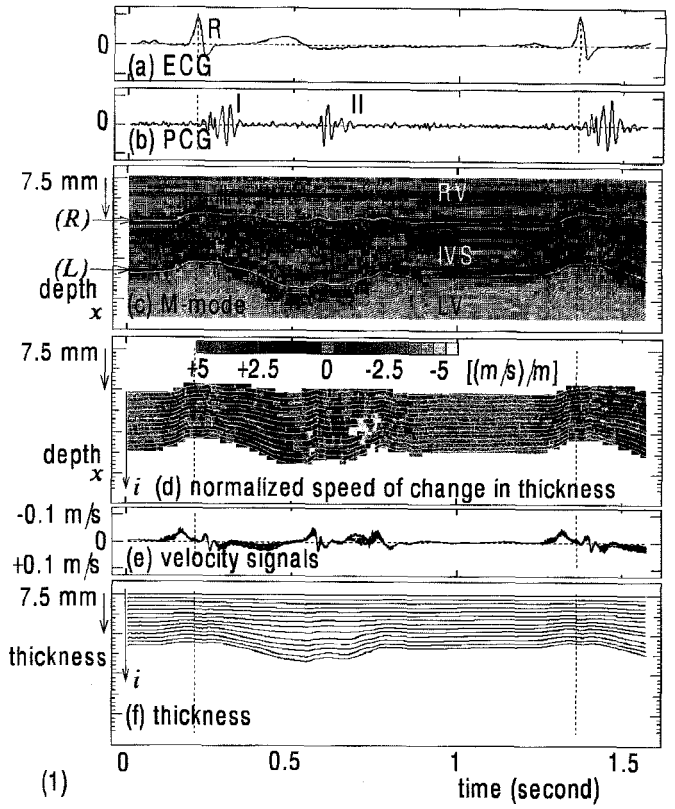

Fig. 6. *In vivo* experimental results of the instantaneous object position and the velocity estimated at 14 points $\{i\}$ in the IVS for the first cardiac cycle. (1) the normal subject in Fig. 5. (2) a 32-year-old male patient with acute lymphoblastic leukemia and with serious cardiomyopathy, who had been treated with antracenadiones, where the measurement was performed five months before his death. (3) the same serious patient as Fig. 6(2), where the measurement was performed two months before his death and three months after the measurement in Fig. 6(2). (a): ECG. (b): PCG. (c): The M-mode image. (d): The tracking results $\{\widehat{x}_i(t)\}$ in (7) of the 14 points $\{i\}$ are shown by white lines. The normalized speed of the change in thickness, $S_i(t)$ [(m/s)/m], is mapped according to the defined color scheme and is superimposed on the tracking results. (e): Superimposed estimates of the velocity signals $\{\widehat{v}(x_i;t)\}$ of the 14 points $\{i\}$ in the heart wall. (f): The change in thickness, $\widehat{x}_i(t) - \widehat{x}_1(t)$, in the region from the RV side to the ith point in the IVS for $i = 1, 2, \ldots, 14$.

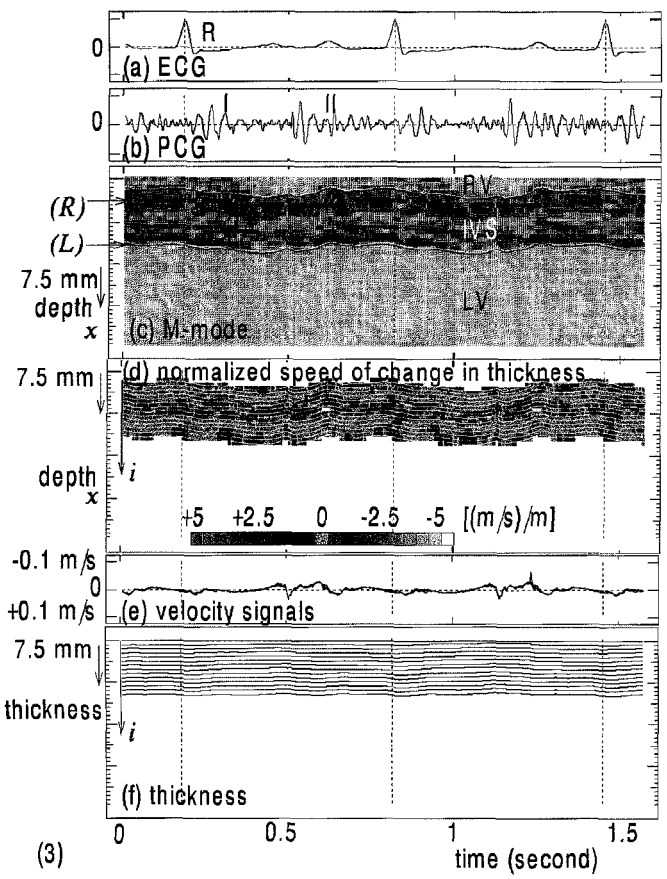

Figs. $\{7(\text{d-}i)\}$ (i=1, 3, 5, 7, 9, 11, 13) show the average power spectra $\{P(x_i;f)\}$ of $\{\widehat{v}(x_i;t)\}$ in Figs. $\{7(\text{c-}i)\}$. Each spectrum is obtained by applying FFT to $\widehat{v}(x_i;t)$ for the period of ± 100 ms around the timing of the second heart sound (II) in Fig. 7(a) for each heartbeat, where the Hanning window is employed. The vertical bar for each frequency shows the minimum and maximum values of the power spectra of the velocity signals in the first five heartbeats. As shown in these figures, there are large components in the low frequency range less than 25 Hz, which correspond to the large motion due to the heartbeats. There is sufficient reproducibility even for the high frequency components from 25 Hz to 90 Hz. The frequency component at 90 Hz is less than the maximum component at 10 Hz by about 20 dB. Even for these small components,

which are within the thickness of the overlaid curves in Figs. {7(c-i)}, the waveform is accurately detected by the proposed method.

By applying the power spectra $\{P(x_i; f)\}$ of the velocity signals $\{\widehat{v}(x_i; t)\}$ detected for the points from the RV surface to near the LV surface in the IVS, there are increases of power from $P(x_1; f)$ to $P(x_{13}; f)$, which are similar to those in the velocity signals in Figs. {7(c-i)} due to the thickening and thinning in the heart wall in the period around the second heart sound (II). However, comparison of the power at each frequency in Figs. {7(d-i)} shows that an increase of power occurs in the frequency band from 25 Hz to about 90 Hz, while for the components in the frequency band less than 25 Hz, there is little difference in power. From these results, the dominant frequency band of the components generated by the thickening and thinning in the heart wall at the timing around the second heart sound, which is shown by red and blue in Fig. 6(1-d), is from 25 Hz to at least 90 Hz.

To *quantitatively* evaluate the reproducibility of the similarity of the M-heartbeat velocity signals $\{\widehat{v}_j(x_i; t)\}$ $(j = 1, 2, \ldots, M)$ for each frequency component of f, where subscript j denotes the cardiac cycle number, the reproducibility function $|\gamma_0(f)|^2$ was introduced in the previous report [1]. The range of $|\widehat{\gamma}_0(f)|^2$ is from 0 to 1. If $|\widehat{\gamma}_0(f)|^2$ is equal to 1, the velocity signals $\{\widehat{v}_j(x_i; t)\}$ in the M heartbeats completely coincide for the frequency component of f. If $|\widehat{\gamma}_0(f)|^2$ is zero, there is no correlation among $\{\widehat{v}_j(x_i; t)\}$ for the frequency components of f. Figs. {7(e-i)} (i=1, 3, 5, 7, 9, 11, 13) show the reproducibility function, $|\gamma_0(f)|^2$, of the velocity signals $\{\widehat{v}(x_i; t)\}$ for the first 5 heartbeats in Figs. {7(c-i)}. The analyzed periods are the same as those in Figs. {7(d-i)}. In each result from Fig. 7(e-1) to Fig. 7(e-13), there is a high correlation between these velocity signals for the 5 heartbeats up to about 100 Hz. Thus, the reproducibility of the velocity signals of each point in the myocardium is quantitatively confirmed.

D. Spectrum Analysis of the Speed of Thickness Change

Figs. 8(c), (d), and (e) show the instantaneous speed $\Delta_t h_i(t) = \widehat{v}(x_{i+2}; t) - \widehat{v}(x_i; t)$ of the change in thickness of (8) for the velocity signals in Fig. 5(f), the magnitude of transfer function $H(x_i \rightarrow x_{i+2}; f)$ from $v(x_i; t)$ to $v(x_{i+2}; t)$, and the squared-magnitude of coherence function $\gamma(x_i \rightarrow x_{i+2}; f)$, respectively, estimated in 6 regions in the IVS. These functions are defined in [1], [38]. In Figs. {8(c-i)} (i=1, 3, 5, 7, 9, 11), the results for the first 5 heartbeats are overlaid and shown. The vertical axis is magnified by 4 to those in Figs. {7(c-i)}. Fig. 8(c-0), bottom left, shows the instantaneous speed of the thickness change $\widehat{v}(x_{14}; t) - \widehat{v}(x_1; t)$ of the IVS. Especially in the systole, there are large thickness changes.

In Figs. {8(d-i)} (i=1, 3, 5, 7, 9, 11), the period analyzed and the window employed are the same as those in Fig. 7. As with the results in Fig. 7(d), for these transfer functions also a large increase in power is found to occur in the frequency band from 25 Hz to 90 Hz. Especially in Fig. 7(d-0), the bottom figure, which shows the magnitude of the transfer function from $\{\widehat{v}(x_1; t)\}$ of the RV surface to $\{\widehat{v}(x_{14}; t)\}$ near the LV surface of the IVS, the results are clearly recognized. The magnitude of the transfer function, which corresponds to the amplitude increase of $\widehat{v}(x_{14}; t)$ to $\widehat{v}(x_1; t)$ due to the thickening of the myocardium, is about 5 dB in the frequency band from 25 Hz to 90 Hz.

In Figs. {8(e-i)} (i=1, 3, 5, 7, 9, 11), the analyzed periods are the same as those in Fig. 8(d). There is a high correlation between these small velocity signals for the first 5 heartbeats up to about 90 Hz.

VII. Regional Myocardial Layer Function in a Patient with Acute Lymphoblastic Leukemia

As an example of noninvasive diagnosis of myocardial damage induced by adriamycin injection, we applied the proposed method to a patient with serious cardiomyopathy.

A. Velocity Signals, Change in Thickness, and Color-Coded Imaging

For a 32-year-old male patient with acute lymphoblastic leukemia, who had been treated with antracenadiones (mitoxantrone) and who suffered from Doxorubicin-cardiotoxicity, the waveforms of the velocity signals, thickness change, and $S_i(t)$ in the IVS are shown in Figs. 6(2) and (3). The subject suffered from severe cardiomyopathy. Three months after the measurement in Fig. 6(2), the measurements were repeated for the same patient (in Fig. 6)(3). About two months after the last measurement, the subject died from the congestive heart failure.

As shown in Figs. 6(2) and (3), the results are quite different from those of the normal subject represented in Fig. 6(1). For the velocity signals in Figs. 6(2-e) and (3-e), the amplitude of the signals, especially for the higher frequency components, are smaller than that of the normal subject. As can be seen from Figs. 6(2-f) and (3-f), there is little change in thickness of the IVS. The maximum values of the change in thickness of the IVS are about 850 μm in Fig. 6(2-f) and 490 μm in Fig. 6(3-f). For the normal subject, however, the value is about 3600 μm as shown in Fig. 6(1-f).

There are also clear differences in the spatial-time distributions of $\{S_i(t)\}$ in Figs. 6(2-d) and (3-d) from those in Fig. 6(1-d). For the normal subject, thickening and/or thinning occur simultaneously in time and homogeneously across the LV wall. For the serious patient, however, the periodic change in each layer thickening with the cardiac cycle disappears and, moreover, the heterogeneous behavior across the LV wall becomes obvious.

B. Spectrum Analysis

Fig. 9 shows the velocity signals, their power spectra, and the reproducibility function, estimated at 7 points in the IVS for the same patient. The measurement was performed two months before his death, the same as that in

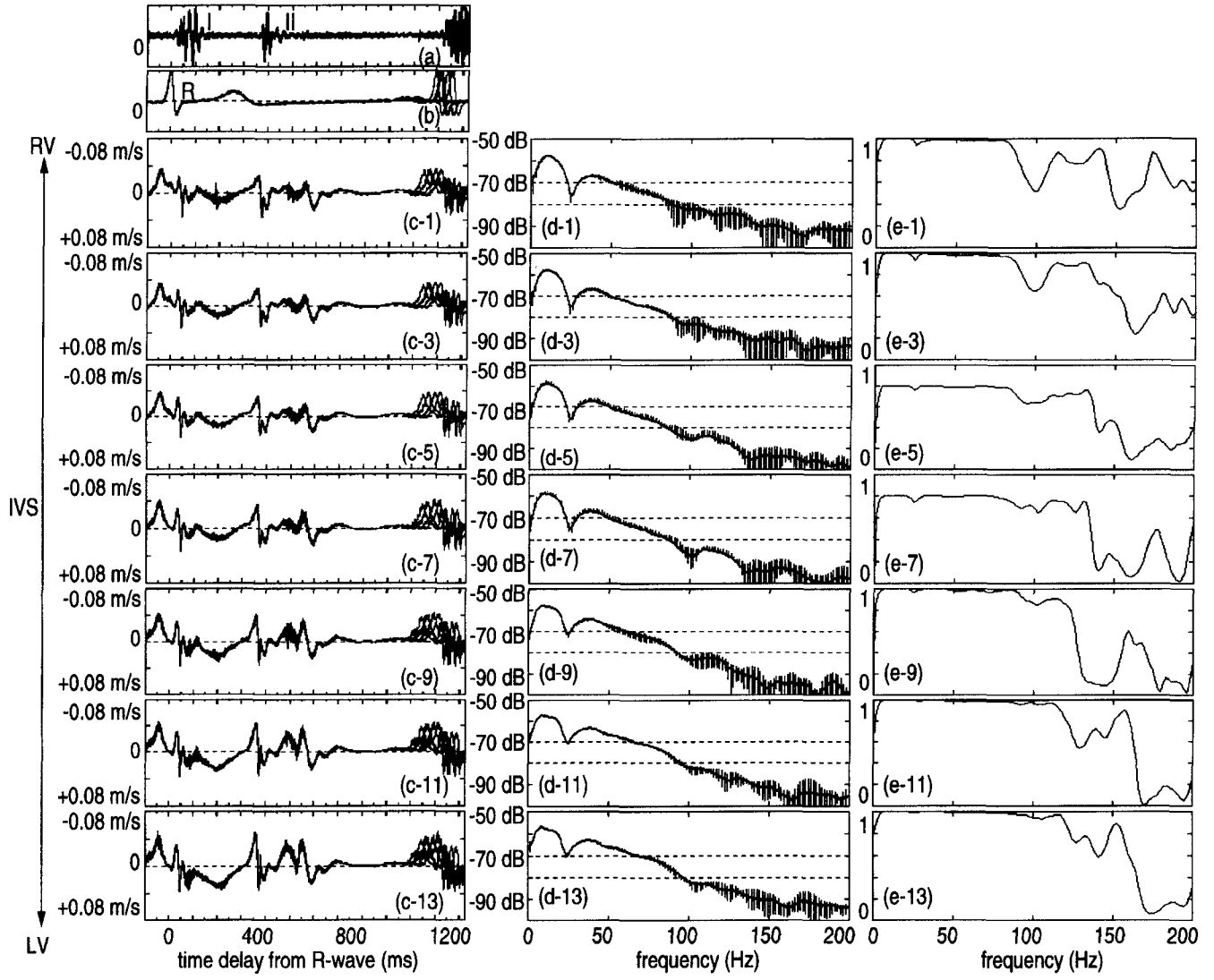

Fig. 7. The velocity signals, their power spectra, and the reproducibility functions, estimated at 7 points in the IVS for the first 5 heartbeats of the normal young male subject in Figs. 4, 5, and 6(1). (a): PCG. (b): ECG. (c-i): the detected velocity signal $\widehat{v}(x_i;t)$ (i=1, 3, 5, 7, 9, 11, 13) at the 7 points from the RV surface to near the LV surface in the IVS. In Figs. (a), (b), and (c), the results for the first 5 heartbeats are overlaid and shown. (d-i): The average power spectrum $P(x_i;f)$ of $\widehat{v}(x_i;t)$ in (c-i). The vertical bar for each frequency shows the minimum and maximum values of the power spectra of the velocity signals in the heartbeats. (e-i): The reproducibility function, $|\gamma_0(f)|^2$, of the velocity signals $\{\widehat{v}(x_i;t)\}$ for the heartbeats in Fig. (c-i). There is a high correlation between these signals for the heartbeats up to about 100 Hz.

Fig. 6(3). By comparing the velocity signals and the power spectra in Figs. 9(c) and (d) with those of the normal subject in Figs. 7(c) and (d), it can be seen that the signal power is greatly decreased, especially for the frequency components higher than 50 Hz. In this frequency band, as described above for the results in Figs. {7(c-i)} for the normal subject, there are large differences of the velocity signals between both sides of the IVS, and these differences generate the thickening and thinning components in the heart wall. For the serious patient, however, the fact that the thickness change of the IVS is not recognized at all corresponds to the lack of the frequency component in this frequency band.

Fig. 10 shows the instantaneous speed $\Delta_t h_i(t)$ of the thickness change of (8), the transfer function $H(x_i \to x_{i+1};f)$ from $v(x_i;t)$ to $v(x_{i+2};t)$, and the squared-magnitude of coherence function, estimated in 6 regions in the IVS for the patient represented in Fig. 6(3). The amplitude of the instantaneous speed $\Delta_t h_i(t)$ of the thickness change for all local regions in the IVS other than the region between the 7th point and 9th point in Fig. 10(c-7) is very small as shown in Fig. 10(c). Regarding the magnitude of the transfer function in Fig. 10(d), the values are almost 0 dB; this means that the components due to the thickening and thinning cannot be recognized.

These differences between the normal subject and the serious patient correspond to the changes in the acoustical characteristics of the local heart wall due to the injection of mitoxantrone. Mitoxantrone has been reported to have an adverse cardiotoxic effect, which results in irreversible diffuse myocardial fibrosis at cumulative or high doses [39]. Taking these experimental results into account, the

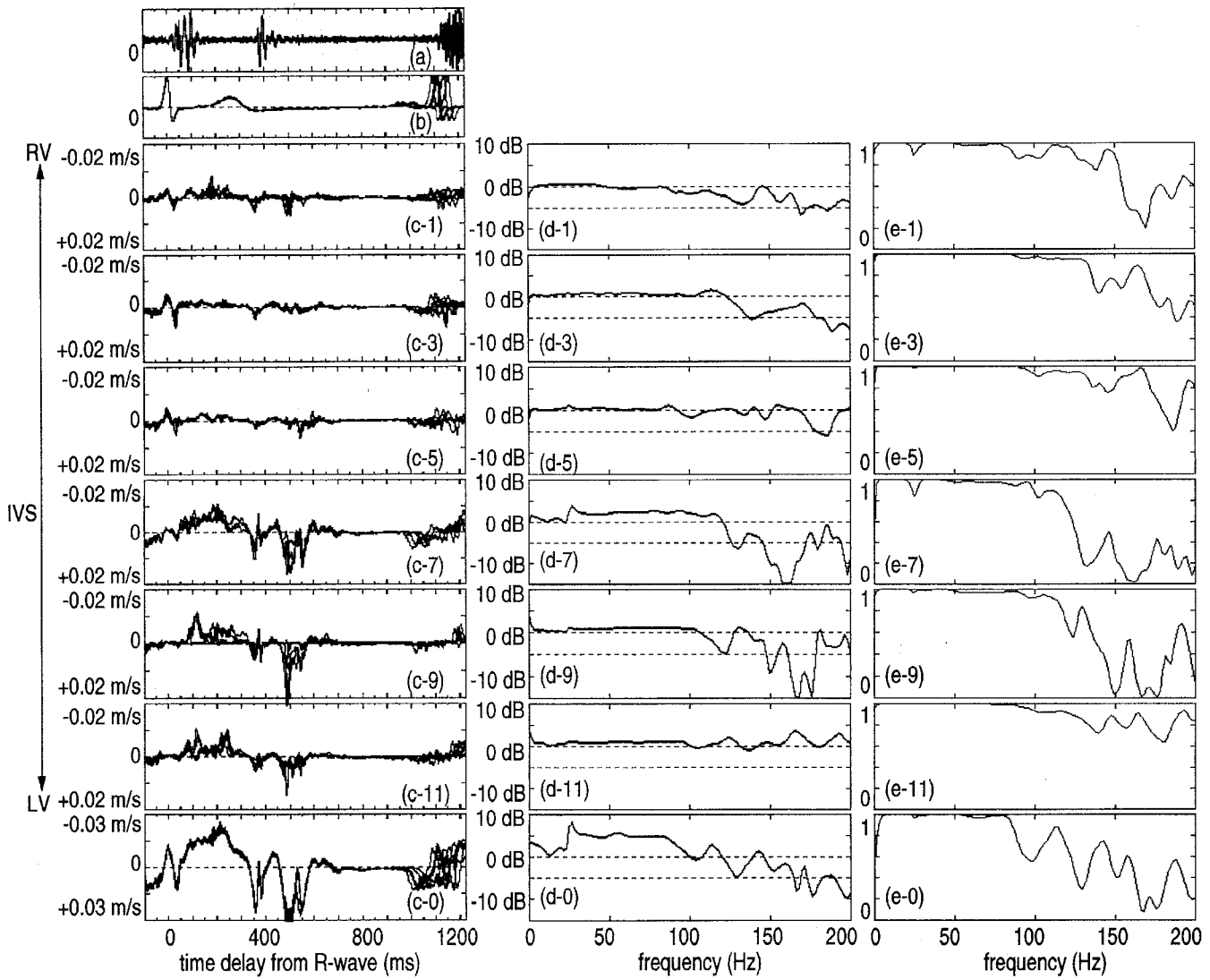

Fig. 8. The instantaneous speed of the thickness change, the transfer function, and the coherence function, estimated in 6 local regions in the IVS for the 5 heartbeats of the normal young male subject in Figs. 4, 5, 6(1), and 7. (a): PCG. (b): ECG. (c-i): The instantaneous speed $\Delta_t h_i(t)$ of the change in thickness, where i=1, 3, 5, 7, 9, 11 in 6 regions preset from the RV surface to the LV surface in the IVS. In (a), (b), and (c), the results for the first 5 heartbeat are overlaid and shown. (d-i): The magnitude of the transfer function $H(x_i \rightarrow x_{i+2}; f)$ from $\widehat{v}(x_i; t)$ to $\widehat{v}(x_{i+2}; t)$ in (c). (e-i): The squared-magnitude of the coherence function, $|\gamma_{i,i+2}(f)|^2$, between signals $\widehat{v}(x_i; t)$ and $\widehat{v}(x_{i+2}; t)$ in (c). (c-0), (d-0), and (e-0): The respective results for the data between $\widehat{v}(x_R; t) = \widehat{v}(x_1; t)$ on the RV surface and $\widehat{v}(x_{14}; t)$ near the LV surface in the IVS.

method proposed in this paper provides a new approach to the detection of such myocardial physical and/or histological heterogeneity by analyzing velocity waveform and the instantaneous local change in thickness of the heart wall detected noninvasively from the chest surface.

VIII. *In Vivo* Experimental Results for LV Posterior Wall

Figs. 11(1) and (2) show the experimental results obtained by applying the proposed method to the LV posterior wall of another 22-year-old male subject and the patient with serious cardiomyopathy in Fig. 6(3), respectively. The latter measurement was performed two months before the patient's death. The 19 points are set at even intervals of $\Delta x_S = 0.75$ mm from the endocardium of the LV posterior wall to the epicardium as shown in Figs. 11(1-d) and (2-d). The ultrasonic beam passing through these points is almost perpendicular to the posterior wall during the measurements. The display format in Figs. 11(1) and (2) is similar to that in Figs. 6(1), (2), and (3). In Figs. 11(1) and (2), however, the maximum value of the vertical axis is 0.15 m/s and the maximum value of 5 [(m/s)/m] of the normalized speed of the thickness change is replaced by 10 [(m/s)/m], since the amplitude of the motion is larger in the posterior free wall. The waveforms of the velocity signals are seen to be quite different from those in the IVS.

From Figs. 11(1-c), (2-c), (1-d), and (2-d), it can be seen that there is parallel motion due to the heartbeat with an amplitude of about 8.6 mm for the normal subject and about 4.5 mm for the patient. For the normal subject

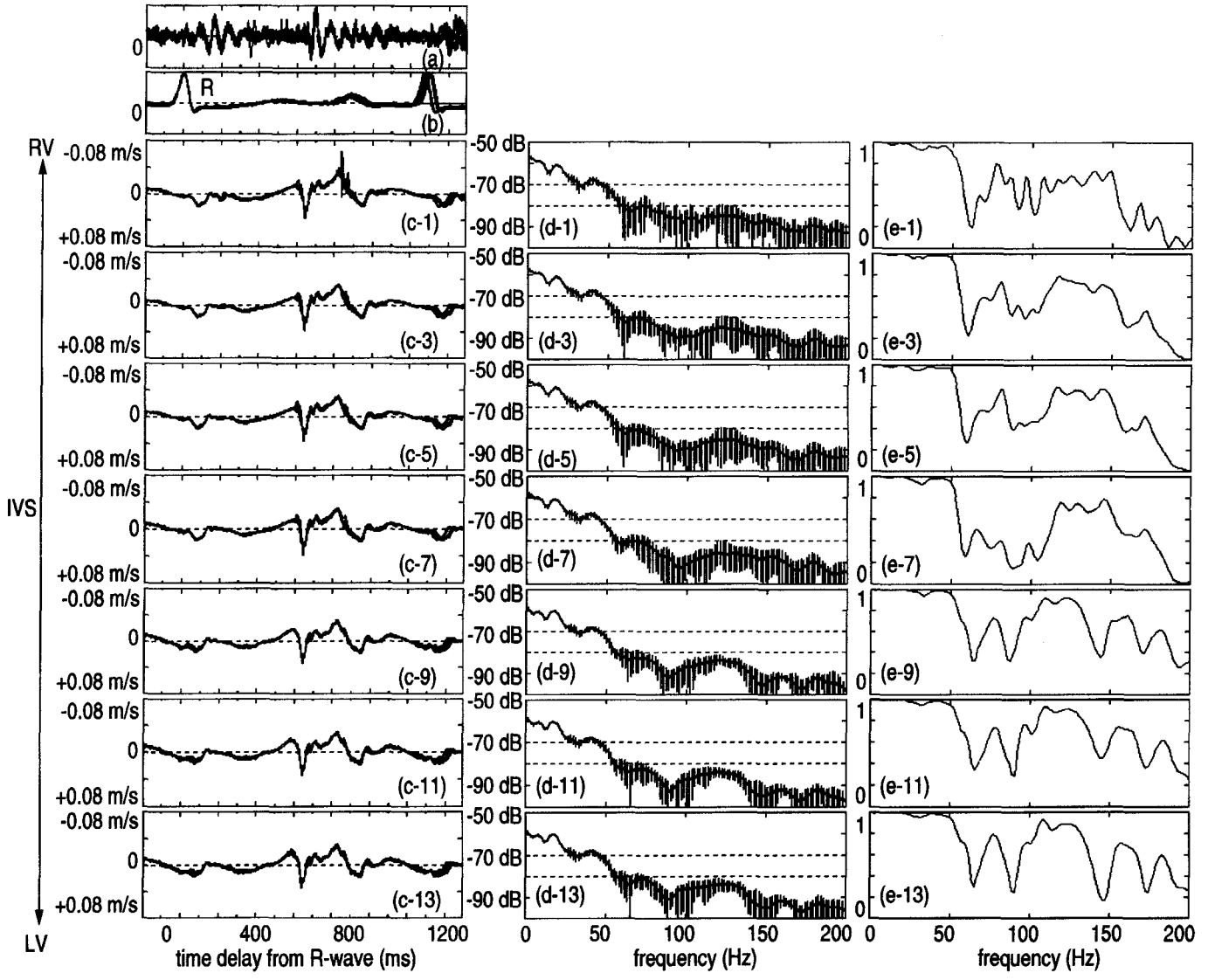

Fig. 9. The velocity signals, their power spectra, and the reproducibility function, estimated at 7 points in the IVS for the 8 heartbeats of the serious patient in Fig. 6(3). The measurement was performed two months before his death. (For details see Fig. 6.)

represented in Fig. 11(1-f), the thickness of the posterior wall is about 12 mm at the end of the diastole and the wall becomes about 6 mm thicker for the systolic phase than that of the diastolic phase. For the serious patient in Fig. 11(2-f), however, the wall becomes only about 3 mm thicker in the systolic phase than in the diastolic phase. At the same time, the normalized speed of the thickness change during the myocardial relaxation for the diastole, which is the gradient of the lines in Fig. 11(1-f), is different from that in Fig. 11(2-f).

IX. Discussion

A. Measurement of Velocity and Displacement

All the techniques for velocity estimation employed in pulse-Doppler systems rely on the relationship of (1) between the phase-shift $\Delta\theta(x_i;t)$ and the displacement $\Delta x_i(t)$ during the interval ΔT of consecutive echoes. To determine the phase-shift $\Delta\theta(x_i;t)$, an efficient complex cross-correlation technique has been developed in [11] for real-time two-dimensional blood flow imaging. Since the cross-correlation is averaged over a duration of about 10 received echoes in the actual system, the time resolution of the resultant waveform is not so high.

The theoretical limitations of the phase-shift measurement are explained in [34] as follows: Variance of the estimation of the phase-shift increases if broadband excitation is employed to improve the range-resolution; and the propagation-attenuation effect introduces the bias error due to the shift of the center frequency in the received echoes. These limitations are also not overcome in our method.

To improve the range-resolution and accuracy of the estimated velocity and overcome the velocity-limitation of the pulse Doppler due to the aliasing effect, the velocity and the displacement are directly estimated by time-shift measurement using the local cross-correlation

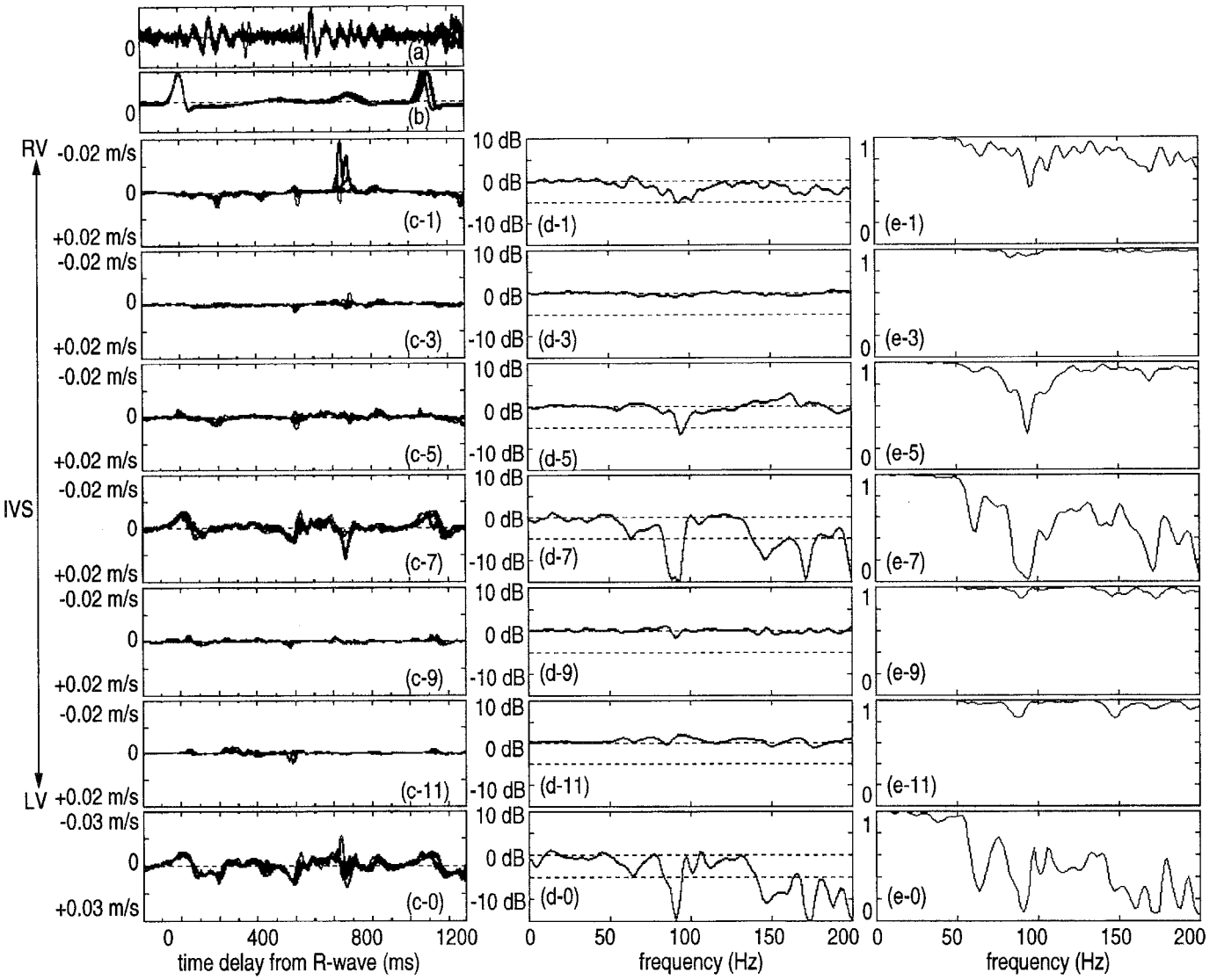

Fig. 10. The instantaneous speed $\Delta_t h_i(t)$ of the thickness change of (10), the transfer function $H(x_i \to x_{i+2}; f)$ from $v(x_i; t)$ to $v(x_{i+2}; t)$, and the coherence function, estimated in 6 regions in the IVS for the 8 heartbeats of the serious patient in Figs. 6(3) and 9. The measurement was performed two months before his death. (For details see Fig. 8.)

between consecutive RF signals in [34]. When the velocity and/or displacement are determined by the cross-correlation function of the RF signal, measurement of displacement of 2 μm would require a very high frequency of 375 MHz (= 1500 [m/s]/(2 [μm] $\times$ 2)). To improve the estimation precision in the cross-correlation function of subsampled RF signals, several interpolation methods have been proposed and their performances are compared in [33]. Reconstruction interpolation, although entailing high computational costs, can decrease bias error in the time delay estimation to subnanoseconds, which corresponds to the displacement of submicrometers. However, a high sampling frequency of about 50 MHz is still required by this interpolation method.

As confirmed by the experiment in Section V, the lowest measurable velocity by our method is about 0.1 mm/s, and the lowest measurable change in thickness and the displacement is about 0.1 μm.

B. Comparison of Color-Coded Imaging Between the Proposed Method and Tissue Doppler Imaging

For the display of the local velocity in the myocardium, tissue Doppler imaging has been already developed [35]–[37]. By this method, the color code determined from the local instantaneous velocity is superimposed on both M-mode and B-mode images. The lowest measurable velocity of the system based on the conventional color Doppler imaging technique is 2 mm/s [37]. Using the same data set of the IVS and the posterior wall of a 23-year-old male with Doxorubicin-cardiotoxicity at complete remission, the normalized speed of the change in thickness obtained by the proposed method and the superimposed M-mode image obtained by the tissue Doppler method are compared in Figs. 12(1) and (2), respectively.

In the results obtained by tissue Doppler imaging shown in Fig. 12(2), the color code of each point in the heart wall

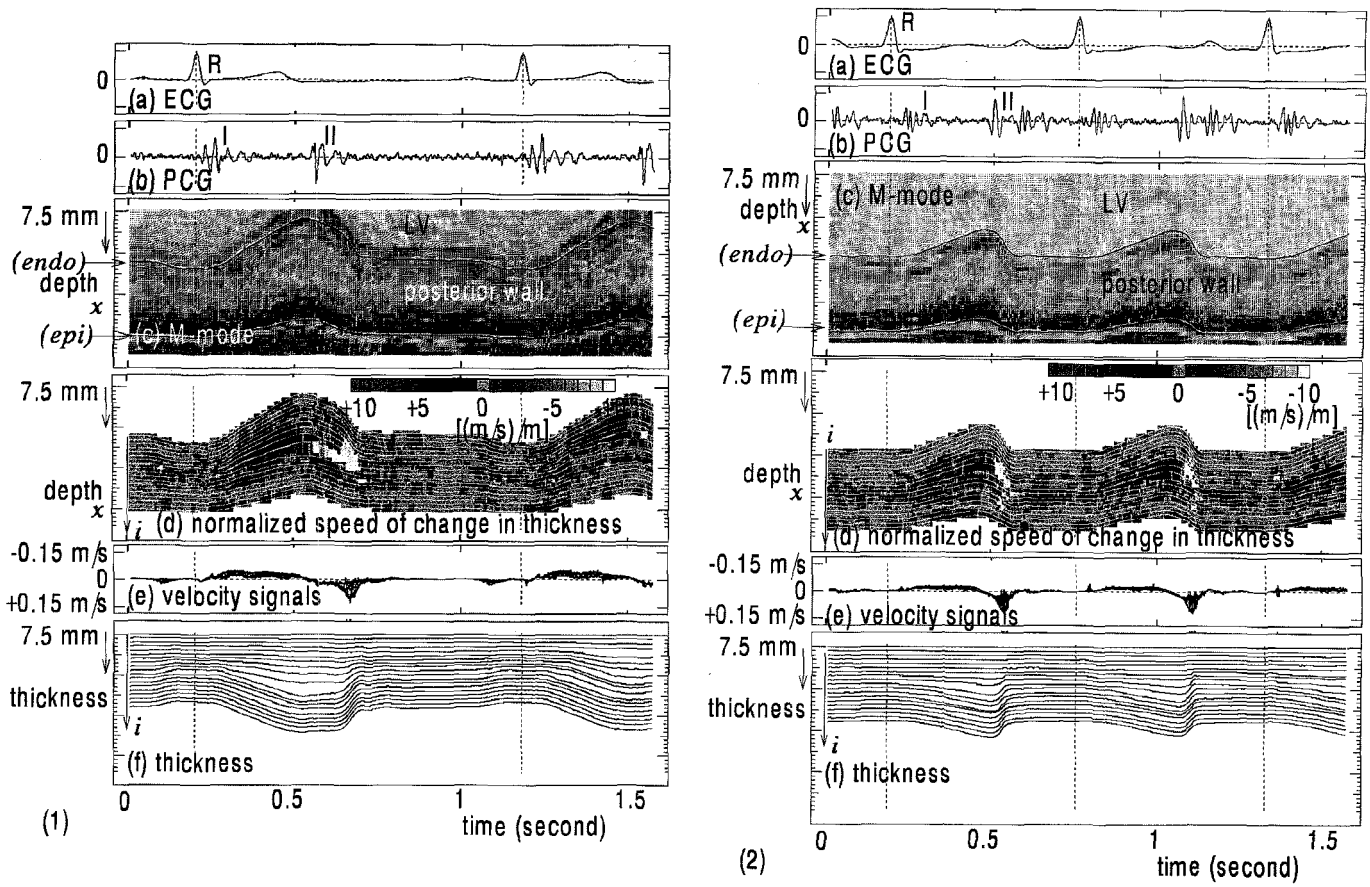

Fig. 11. *In vivo* experimental results of the instantaneous object position and the velocity estimated at 19 points $\{i\}$ in the posterior wall of another normal subject (1) and the same serious patient (2) as Fig. 6(3), where the measurement was performed two months before his death.. (a): ECG. (b): PCG. (c): The M-mode image. Two white lines show the estimated instantaneous positions $\widehat{x_1}(t) = \widehat{x_R}(t)$ and $\widehat{x_{19}}(t) = \widehat{x_L}(t)$ on the endocardium and the epicardium, respectively. (d): The tracking results $\{\widehat{x_i}(t)\}$ in (7) of the 19 points $\{i\}$ are shown by white lines. The normalized speed of the change in thickness, $S_i(t)$ [(m/s)/m], is mapped according to the defined color scheme and is superimposed on the tracking results. (e): Superimposed estimates of the velocity signals $\{\widehat{v}(x_i;t)\}$ of the 19 points $\{i\}$ in the heart wall. (f): The change in thickness, $\widehat{x_i}(t) - \widehat{x_1}(t)$, in the region from the endocardium to the ith point in the posterior wall for $i = 1, 2, \ldots, 19$.

is determined by the velocity and its polarity. Namely, it is determined by *the sum of the parallel global motion and the local change in thickness.* However, since the amplitude of the parallel global motion is dominant, the spatial distribution of the velocity in the IVS and the posterior wall is not so clear, that is, the image reflects the global motion of the LV wall relative to the precordial probe, but not the myocardial layer thickening/thinning across the LV wall.

For the normalized speed of the change in thickness obtained by the proposed method, however, the parallel global motion with large amplitude induced by the cardiac beat is canceled and, consequently, the color code on the M-mode image discriminates the instantaneous change in thickness in the local area around each point as shown in Fig. 12(1). The noninvasive evaluation of spatial distribution of speed of local myocardial thickening/thinning has not been realized in the conventional ultrasonic diagnosis systems, and the proposed method has the potential to provide information relative to the noninvasive diagnosis of myocardial local motility.

C. Advantages of the Proposed Method for Spectrum Analysis

The velocity signal measurement by the proposed method has the following advantages compared with the conventional methods.

1. The measurable frequency band is from d.c. to several hundred Hz. Since components in the frequency band higher than 100 Hz in the velocity signal of the heart wall are not large, the velocity signals of the frequency band, at least until 100 Hz, are accurately measured with sufficient reproducibility.

2. With standard Doppler equipment and in almost all the methods, including the wall-tracking techniques reported in the literature, the measured velocity and/or the displacement are displayed in the time domain. The effective frequency band is less than 20 Hz and the frequency components from 20 Hz to 100 Hz are not considered. As shown in Fig. 8(d-0), however, the dominant component of the change in thickness is in this frequency band. Thus, for the accurate detection of the change in thickness of the

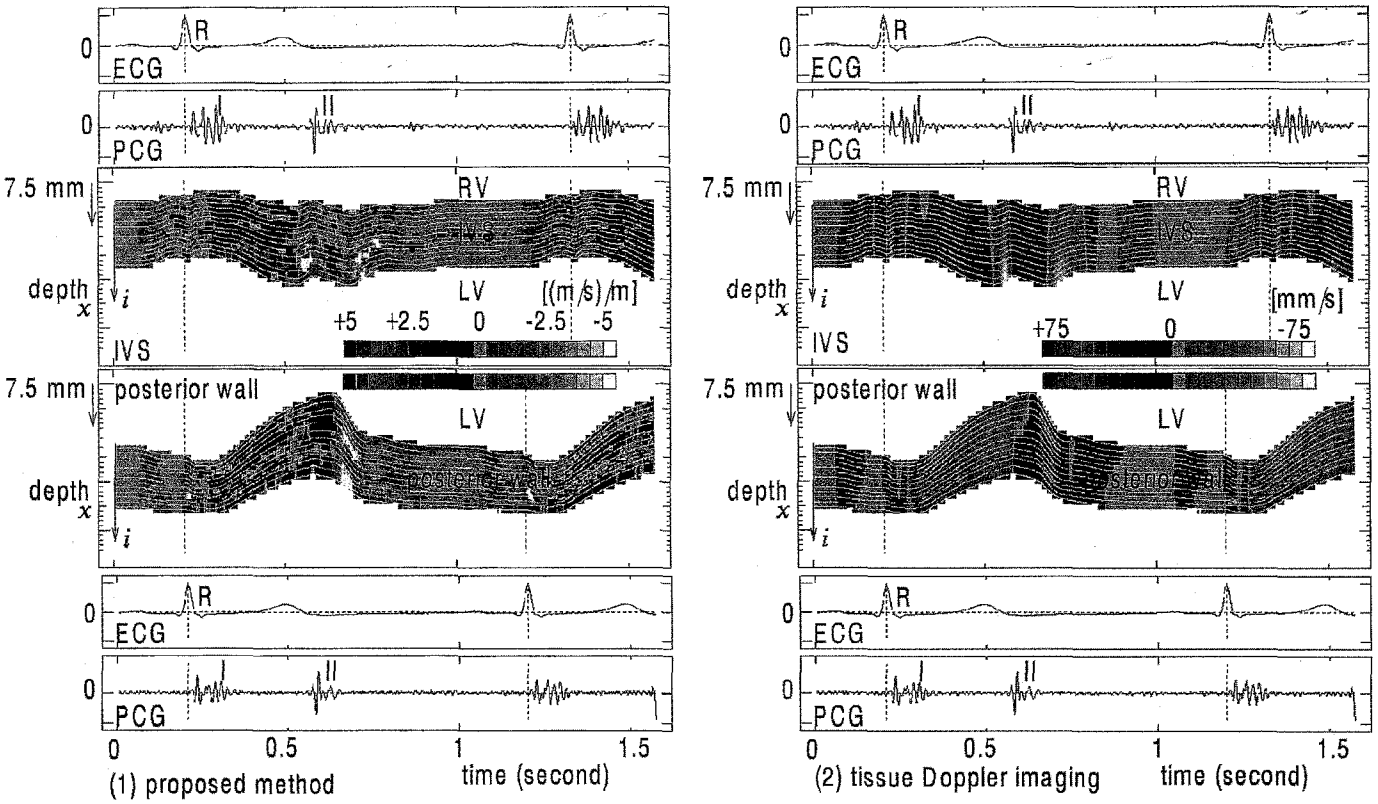

Fig. 12. *In vivo* experimental results obtained by the proposed method (1) and the tissue Doppler imaging (2) at multiple points $\{i\}$ in the IVS and the posterior wall of a 23-year-old male patient with mild cardiomyopathy. The tracking results $\{\hat{x}_i(t)\}$ in (7) of the multiple points $\{i\}$ are shown by white lines. (1): The normalized speed of the change in thickness, $S_i(t)$ [(m/s)/m], is mapped according to the defined color scheme and is superimposed on the tracking results. (2): The velocity, $v(x_i;t)$ [(m/s)], is mapped according to the defined color scheme and is superimposed on the tracking results.

myocardium, it is essential to measure such high frequency components; our method is the first to achieve this.

3. As evaluated in Section V, the proposed method has a wide dynamic range of about 73 dB, the spectrum analysis being applied even for frequency band higher than 20 Hz to 100 Hz, where the amplitude of the frequency components is very small, i.e., several micrometers. These high frequency components with small amplitude are also accurately measured by our method with sufficient reproducibility.

X. Conclusions

In this paper we have proposed a new noninvasive method for evaluation of local thickness change in the heart wall using ultrasound. By an *in vivo* measurement system to realize this method, both the instantaneous positions and the velocity signals of the multiple points preset in the heart wall are accurately detected in the frequency range up to 100 Hz with sufficient reproducibility. By color-coded imaging, moreover, the spatial-time distribution of the instantaneous local change in thickness of the heart wall are obtained. For a serious patient, the results are quite different from those of the normal subject. From the difference in the power spectra of the velocity signals at multiple points in the heart wall, the frequency band where the myocardial expansion and contraction occur is identified. From the spectrum analysis of the velocity signal of the serious patient, the components in this frequency band are greatly decreased.

Since these preliminary studies in this paper were performed in young patients with clear echocardiograms, much work must be done to find out how the method can be applied in a wider range of subjects and to see whether it can contribute to assessment of myocardial diseases and recovery. Further investigation of this proposed method, including its clinical application to the noninvasive local diagnosis of coronary artery disease, drug-induced myocardial disease, and arteriosclerosis of patients including elder subjects, is being conducted. It will be necessary to compare the *in vivo* results obtained herein by the proposed method with pathological findings in order to evaluate the range of variability in clinical studies and construct a standard which can be applied to the *in vivo* diagnosis of the heart wall.

The direction of the ultrasonic beam was selected so that the beam was perpendicular to the heart wall in this paper. It is necessary to overcome the limitation. It will also be necessary to identify the origin of the parallel global motion detected in this paper. In this study, detected velocity signals were analyzed in the frequency domain only for the period around the second heart sound emission. It

will also be necessary to analyze the velocity signals for other periods, including systole and the end of diastole.

ACKNOWLEDGMENTS

The authors are grateful to Prof. Floyd Dunn of the Bioacoustics Research Laboratory, the University of Illinois, and Prof. Kunio of Shirato of Tohoku University School of Medicine for discussions and encouragement and to Associate Prof. Yoshiko Saito, Prof. Fumiaki Tezuka, and Dr. Eiichi Kamata of Tohoku University School of Medicine for helpful discussion and assistance with experiments. The authors also acknowledge the contributions of Michie Sato, Kohshiro Sugimura, and Shigemitsu Nakaya in our laboratory.

REFERENCES

[1] H. Kanai, M. Sato, Y. Koiwa, and N. Chubachi, "Transcutaneous measurement and spectrum analysis of heart wall vibrations," *IEEE Trans. Ultrason., Ferroelect., Freq. Contr.*, vol. 43, pp. 791–810, Sept. 1996.

[2] S. Satomura, "Ultrasonic Doppler method for the inspection of cardiac function," *J. Acoust. Soc. Amer.*, vol. 29, pp. 1181–1185, Nov. 1957.

[3] D. W. Baker, "Pulsed ultrasonic Doppler blood-flow sensing," *IEEE Trans. Sonics Ultrason.*, vol. SU-17, pp. 170–185, July 1970.

[4] F. D. McLeod and M. Anliker, "A multiple-gate pulsed directional Doppler flowmeter," *Proc. IEEE Ultrason. Symp.*, Dec. 1971.

[5] S. L. Johnson, D. W. Baker, R. A. Lute, and H. T. Dodge, "Doppler echocardiography," *Circulation*, vol. XLVIII, pp. 810–822, Oct. 1973.

[6] F. E. Barber, D. W. Baker, A. W. C. Nation, D. E. Strandness, Jr., and J. M. Reid, "Ultrasonic duplex echo-Doppler scanner," *IEEE Trans. Biomed. Eng.*, vol. BME-21, pp. 109–113, Mar. 1974.

[7] C. J. Hartley, H. G. Hanley, R. M. Lewis, and J. S. Cole, "Synchronized pulsed Doppler blood flow and ultrasonic dimension measurement in conscious dogs," *Ultras. Med. Biol.*, vol. 4, pp. 99–110, 1978.

[8] M. Brandestini, "Topoflow—A digital full range Doppler velocity meter," *IEEE Trans. Sonics Ultrason.*, vol. SU-25, pp. 287–293, Sept. 1978.

[9] E. Wildi, J. W. Knutti, H. V. Allen, and J. D. Meindl, "Dynamics and limitations of blood/muscle interface detection using Doppler power returns," *IEEE Trans. Biomed. Eng.*, vol. BME-27, pp. 565–573, Oct. 1980.

[10] W. D. Barber, J. W. Eberhard, and S. G. Karr, "A new time domain technique for velocity measurements using Doppler ultrasound," *IEEE Trans. Biomed. Eng.*, vol. BME-32, pp. 213–229, Mar. 1985.

[11] C. Kasai, K. Namekawa, A. Koyama, and R. Omoto, "Real-time two-dimensional blood flow imaging using an autocorrelation technique," *IEEE Trans. Sonics Ultrason.*, vol. SU-32, pp. 458–463, May 1985.

[12] R. M. Olson and D. K. Shelton, "A nondestructive technique to measure wall displacement in the thoracic aorta," *J. Appl. Phys.*, vol. 32, pp. 147–151, Jan. 1972.

[13] R. M. Olson and J. P. Cooke, "A nondestructive ultrasonic technique to measure diameter and blood flow in arteries," *IEEE Trans. Biomed. Eng.*, vol. BME-21, pp. 168–171, 1974.

[14] J. O. Arndt, "The diameter of the intact carotid artery in man and its change with pulse pressure," *Pflüegers Arch.*, vol. 301, pp. 230–240, 1968.

[15] D. J. Mozersky, D. S. Sumner, D. E. Hokanson, and D. E. Strandness, Jr., "Transcutaneous measurement of the elastic properties of the human femoral artery," *Circulation*, vol. XLVI, pp. 948–955, Nov. 1972.

[16] A. P. G. Hoeks, C. J. Ruissen, P. Hick, and R. S. Reneman, "Transcutaneous detection of relative changes in artery diameter," *Ultras. Med. Biol.*, vol. 11, no. 1, pp. 51–59, 1985.

[17] W. T. Kemmerer, R. W. Ware, H. F. Stegall, J. L. Morgan, and R. Kirby, "Blood pressure measurement by Doppler ultrasonic detection of arterial wall motion," *Surg. Gynec. Obstet.*, vol. 131, pp. 1141–1147, Dec. 1970.

[18] K. Lindström, K. Marsal, G. Gennser, L. Bengtsson, M. Benthin, and P. Dahl, "Device for measurement of fetal breathing movements. 1. The TD-recorder. A new system for recording the distance between two echogenerating structures as a function of time," *Ultras. Med. Biol.*, vol. 3, pp. 143–151, 1977.

[19] D. E. Hokanson, D. E. Strandness, Jr., and C. W. Miller, "An echo-tracking system for recording arterial wall motion," *IEEE Trans. Sonics Ultrason.*, vol. SU-17, pp. 130–132, July 1970.

[20] D. E. Hokanson, D. J. Monzersky, S. D. Sumner, and D. E. Strandness, Jr., "A phase-locked echo tracking system for recording arterial diameter changes *in vivo*," *J. Appl. Phys.*, vol. 32, pp. 728–733, May 1972.

[21] K. Nakayama and S. Sato, "Ultrasonic measurement of arterial wall movement utilizing phase-tracking system," *Digest, 10th Int. Conf. Med. Biol. Eng.*, Dresden, 1973, p. 318.

[22] D. N. White and R. J. Stevenson, "Transient variations in the systolic pulsations in amplitude of intracranial echoes, their artificial origin," *Neurology*, vol. 26, pp. 683–689, 1976.

[23] C. F. Olsen, "Doppler ultrasound: a technique for obtaining arterial wall motion parameters," *IEEE Trans. Sonics Ultrason.*, vol. SU-24, pp. 354–358, June 1977.

[24] L. W. Korba, R. S. C. Cobbold, and A. J. Cousin, "An ultrasonic imaging and differential measurement system for the study of fetal respiratory movements," *Ultras. Med. Biol.*, vol. 5, pp. 139–149, 1979.

[25] I. Rapoport and A. J. Cousin, "New phase-lock tracking instrument for foetal breathing monitoring," *Med. Biol. Eng. Comput.*, vol. 20, pp. 1–6, Jan. 1982.

[26] D. H. Groves, T. Powalowski, and D. N. White, "A digital technique for tracking moving interfaces," *Ultras. Med. Biol.*, vol. 8, no. 2, pp. 185–190, 1982.

[27] C. J. Hartley, H. Litowitz, R. S. Rabinovitz, W. X. Zhu, J. E. Chelley, L. H. Michael, and R. Bolli, "An ultrasonic method for measuring tissue displacement: technical details and validation for measuring myocardial thickening," *IEEE Trans. Biomed. Eng.*, vol. BME-38, pp. 735–747, Aug. 1991.

[28] L. S. Wilson and D. E. Robinson, "Ultrasonic measurement of small displacements and deformations of tissue," *Ultrason. Imag.*, vol. 4, pp. 71–82, 1982.

[29] C. J. Hartley, L. A. Latson, L. H. Michael, C. L. Seidel, R. M. Lewis, and M. L. Entman, "Doppler measurement of myocardial thickening with single epicardial transducer," *Amer. J. Physiol.*, vol. 245, pp. H1066–1072, 1983.

[30] A. P. G. Hoeks, P. J. Brands, F. A. M. Smeets, and R. S. Reneman, "Assessment of the distensibility of wuperficial arteries," *Ultras. Med. Biol.*, vol. 16, no. 2, pp. 121–128, 1990.

[31] R. W. Stadler, W. C. Karl, and R. S. Lees, "The Application of echo-tracking methods to endothelium-dependent vasoreactivity and arterial compliance measurements," *Ultras. Med. Biol.*, vol. 22, no. 1, pp. 35–42, 1996.

[32] H. Kanai, H. Satoh, K. Hirose, and N. Chubachi, "A new method for measuring small local vibrations in the heart using ultrasound," *IEEE Trans. Biomed. Eng.*, vol. 40, pp. 1233–1242, 1993.

[33] I. Céspedes, Y. Huang, J. Ophir, and S. Spratt, "Methods for estimation of subsample time delays of digitized echo signals," *Ultrason. Imag.*, vol. 17, no. 2, pp. 142–171, 1995.

[34] O. Bonnefous and P. Pesqué, "Time domain formulation of pulse-Doppler ultrasound and blood velocity estimation by cross-correlation," *Ultrason. Imag.*, vol. 8, no. 2, pp. 73–85, 1986.

[35] W. N. McDicken, G. R. Sutherland, C. M. Moran, and L. N. Gordon, "Color Doppler velocity imaging of the myocardium," *Ultras. Med. Biol.*, vol. 18, nos. 6/7, pp. 651–654, 1992.

[36] K. Miyatake, N. Tanaka, M. Yamagishi, N. Yamazaki, Y. Mine, and M. Hirama, "Clinical application of newly developed color coded tissue Doppler echocardiography in detection of abnormal ventricular wall motion," *J. Amer. Soc. Echocardiography*, vol. 6, Part 2, p. S19, May-June 1993.

[37] N. Yamazaki, Y. Mine, A. Sano, M. Hirama, and K. Miyatake, "Analysis of ventricular wall motion using color-coded tissue Doppler imaging system," *Jpn. J. Appl. Phys.*, vol. 33, no. 5B, pp. 3141–3146, 1994.

[38] J. A. Cadzow and O. M. Solomon, Jr., "Linear modeling and the coherence function," *IEEE Trans. Acoust., Speech, Sig. Proc.*, vol. 35, no. 1, pp. 19–28, 1987.
[39] J. Dunn, "Doxorubicin-induced cardiomyopathy," *J. Pediatr. Oncol. Nurs.*, vol. 11, no. 4, pp. 152–160, 1994.

Hiroshi Kanai (A'88–M'91) was born in Matsumoto, Japan, on November 29, 1958. He received a B.E. degree from Tohoku University, Sendai, Japan in 1981, and M.E. and the Ph.D. degrees, also from Tohoku University, in 1983 and in 1986, both in electrical engineering.

From 1986 to 1988 he was with the Education Center for Information Processing, Tohoku University, as a research associate. From 1990 to 1992 he was a lecturer at the Department of Electrical Engineering, Faculty of Engineering, Tohoku University. Since 1992 he has been an Associate Professor at the Department of Electrical Engineering, Faculty of Engineering, Tohoku University. His present interest is in ultrasonic measurements and digital signal processing for diagnosis of the heart diseases and arteriosclerosis.

Dr. Kanai is a member of the Acoustical Society of Japan, the Institute of Electronics Information and Communication Engineering of Japan, the Japan Society of Mechanical Engineers, the Japan Society of Ultrasonics in Medicine, Japan Society of Medical Electronics and Biological Engineering, the Institute of Electrical Engineers of Japan, the Japanese Circulation Society, and the Japanese College of Cardiology.

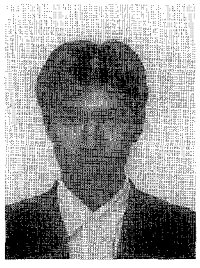

Hideyuki Hasegawa was born in Tochigi, Japan, on August 28, 1973. He received a B.E. degree in electrical engineering from Tohoku University, Sendai, Japan, in 1996.

Since 1996, he has been a postgraduate student of the Department of Electrical and Communication Engineering, Tohoku University, Japan. His current interest is in digital signal processing and ultrasonic measurement for cardiovascular disease and atherosclerosis.

Mr. Hasegawa is a member of the Acoustical Society of Japan, and the Institute of Electrical Engineers of Japan.

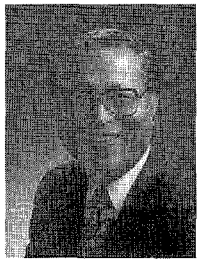

Noriyoshi Chubachi (M'83) received B.S., M.S., and Ph.D. degrees in electrical engineering from Tohoku University, Sendai, Japan, in 1956, 1962, and 1965, respectively.

In 1965, he joined the Research Institute of Electrical Communication, Tohoku University, where he was an associate professor from 1966 to 1978. Since 1979 he has been a professor at the Department of Electrical Engineering, Tohoku University. From 1982 to 1983 he was a visiting Professor of Electrical and Computer Engineering, University of California, Santa Barbara, CA. He has worked on ultrasonic transducers and delay lines, surface acoustic devices, acoustoelectronics, piezoelectric materials, acoustic microscopy, and related problems.

Dr. Chubachi is a member of the Acoustical Society of America, the Institute of Electronics and Communication Engineers of Japan, the Society of Japanese Applied Physics, the Acoustical Society of Japan, the Japan Society of Ultrasonics in Medicine, the Japan Society for Nondestructive Inspection, the Japan Society of Medical Electronics and Biological Engineering, the Japan Society of Mechanical Engineers, and the Institute of Electrical Engineers of Japan. He served as chairman of the Tokyo Chapter of IEEE UFFC Society from 1987 to 1988. He is currently serving as Vice-President of the Acoustical Society of Japan.

Yoshiro Koiwa was born in Sendai, Japan, in 1944. He graduated from Tohoku University, Sendai, Japan, in 1969. He received his M.D. degree from Tohoku University in 1977.

He is presently Associate Professor of First Department of Internal Medicine of Tohoku University. His main research interest is cardiovascular disease, especially cardiac function and heart failure.

Dr. Koiwa is member of American Federation for Clinical Research, the Japanese Circulation Society, the Japan Society of Ultrasonics in Medicine, and the Japan Society of Medical Electronics and Biological Engineering.

Motonao Tanaka was born in Japan in 1932. He received M.D. and the Ph.D. degrees in medical science from Tohoku University, Sendai, Japan, in 1959 and 1963, respectively. He was with the Research Institute for Chest Diseases and Cancer, Tohoku University from 1959 to 1993 and with the Institute of Development, Aging and Cancer from 1993 to 1994, where he was a Professor of Medicine and head of the Department of Medical Engineering and Cardiology. Since 1994 Dr. Tanaka has been the President of Tohoku Welfare Pension Hospital. His research interests are ultrasonics in medicine and cardiology, especially cardiac function and tissue characterization.

Dr. Tanaka is a member of World Federation for Ultrasound in Medicine and Biology, the Japanese College of Cardiology, the Japan Society of Ultrasonics in Medicine, the Acoustical Society of Japan, and the Japan Society of Medical Electronics and Biological Engineering.